Sponsored by
Advanced Research Projects Agency (DOD)
ARPA Order No. 3291

ARPA Order 3291
Program Code 7F10
Name of Grantee: University of Colorado
Effective Date of Grant: 1 November 1974
Grant Expiration Date: 31 October 1977
Amount of Grant: $258,016
Grant Number: AFOSR-75-2775
Principal Investigator: Carl Kisslinger (303) 492-7943
Program Manager: William J. Best
Title of Work: Earthquake Characteristics and Earthquake-Explosion Discrimination

Semi-Annual Technical Report No. 5
1 November 1976 - 30 April 1977

C. Kisslinger, C.B. Archambeau, V.F. Cormier
G. Lundquist, C. Salvado, J. Stevens

APPROVED FOR PUBLIC RELEASE: DISTRIBUTION UNLIMITED.

TABLE OF CONTENTS

TECHNICAL REPORT SUMMARY

The principal effort during the period covered by this report has been directed to developing more thorough understanding of the proper way to account for the effects of the properties of the real Earth on the amplitudes and spectra of seismic body waves. The results of these studies will contribute to the further development of procedures for determining the energy released at the source and the mechanics of the source from the body-waves observed at large distances.

1. A full-wave theory applicable to the synthesis of body-waves at epicentral distances of 10° to 40°, for propagation through an upper mantle with either first-order discontinuities or intense but continuous variations in elastic properties has been developed. The theory for discontinuous velocity changes has been applied to the synthesis of SH waves for an Earth with discontinuities in density and velocity at depths of 420 km and 670 km. Arrivals with decreasing amplitudes at distances beyond the cusps predicted by geometric ray theory are clearly shown.

One way of modeling a region of rapidly changing properties is by the use of a large number of thin homogeneous layers. This approach requires a lengthy calculation of reflection-transmission coefficients. The use of higher-order Langer approximations of the radial eigenfunctions leads to a more efficient technique for treating this problem. When a region of strong gradients in physical properties is sufficiently far from the source and receiver, the scattering caused by the region results in waves arriving at points far from the receiver or at times removed from the arrival time of the transmitted wave. The resulting reduction in amplitude of P and SV waves represents a strong non-anelastic attenuation.

2. An attempt has been made to resolve a portion of the frequency dependence of Q^{-1} using P and S body-wave spectra from shallow and deep earthquakes. Various theories of specific dissipation mechanisms and of the anelastic attenuation correction of body waves have been reviewed. Under the structure of those theories, a model of $Q^{-1}(f)$ is proposed in which Q^{-1} is constant at low frequencies but decays beyond a high frequency cutoff which is a model parameter. The model is tested by assuming high frequency spectral decay slopes of both ω^{-2} and ω^{-3}. P and S waves are tested independently, and a decay in the absorption spectrum is found for both. However, the required modulation is not the same for the two wave types, suggesting the existence of a bulk-loss mechanism which attenuates a narrow range of P-wave frequencies. The depth dependence of $Q^{-1}(f)$ shows that the bulk-loss mechanism is concentrated almost entirely in the asthenosphere, while the shear loss mechanisms are distributed in a complex way throughout the mantle.

3. Two applications of elastodynamic Green's functions have been developed. First, the Green's function representation of a wave field is used to generate an equivalent elastic field that analytically reproduces the field identical to the numerical representation. Then this analytical representation can be used easily and efficiently to predict the further propagation of the field to long distances. The second application uses the Green's function representation to effect a transparent grid boundary for numerical program calculations.

1. BODY-WAVE SYNTHESIS AT 10°-40°

V.F. Cormier

Upper Mantle with First-Order Discontinuities

Introduction

Theoretical seismograms enable the amplitude and waveform of body waves to be incorporated as constraints in an inversion scheme for an earth model or the source time function of an earthquake or explosion. The lower mantle has long been known from travel time studies to be nearly laterally homogeneous and to have elastic moduli and density gradients that vary smoothly and slowly over large ranges of depth. Consequently, in the distance range 40-80° simple geometric ray theory that includes surface reflections combined with a simple source description is sufficient to synthesize the observed waveform of body waves (Herrmann, 1975). At shorter distances, however, geometric ray theory must be abandoned in favor of a full wave theory that includes non-ray theoretical effects of waves grazing regions in the upper mantle and crust having discontinuous and/or rapid variations in velocity and density.

Theoretical seismograms incorporating such a full wave theory can be generated by a variety of methods, but in general all start with a representation of the form

$$u(\Delta_o,t) = \frac{1}{\pi}\int_0^\infty \omega^{1/2}\,\mathrm{Re}\left[\int_\Gamma f\, e^{i\omega J}\,dp\, e^{-i\omega t}\right] d\omega \qquad (1.1)$$

Eq. 1.1 is appropriate for an explosive point source observed at the earth's surface at distance Δ_o and time t, where Γ is a path in the complex ray parameter (p) plane, f is a product of reflection-transmission

coefficients and the source-receiver directivity function, and $J(p,\Delta_o)$ is the phase delay factor.

The phase delay factor is related to the travel time and distance integrals by

$$J(p,\Delta_o) = T(p) - p\Delta(p) + p\Delta_o \tag{1.2}$$

More specifically the phase delay factor is given by

$$J(p,\Delta_o) = \int_{r_p}^{r_s} [1/\alpha^2(r) - p^2/r^2]^{1/2}\, dr + \int_{r_p}^{r_o} [1/\alpha^2(r) - p^2/r^2]^{1/2}\, dr + p\Delta_o \tag{1.3}$$

where r_o is the radius of the receiver, r_s the radius at the source, r_p the radius at which the integrand vanishes, and the integrand is related to the cosine of the angle of incidence by

$$[1/\alpha^2(r) - p^2/r^2]^{1/2} = \cos i/\alpha(r) \tag{1.4}$$

Thus the radius r_p is the turning point radius, that radius where the ray bottoms and $\cos i = 0$.

Fuchs and Müller's (1971) reflectivity method converts the integral over the ray parameter to one over real angles of incidence in which the curvature and radial heterogeneity of the earth is modeled by a stack of homogeneous flat layers, the factor f representing the effect of the infinite set of multiple reflections possible in the layer stack. Some

methods obtain a solution in the time domain by directly operating with Eq. 1.1. The Cagniard method for a sphere (Gilbert and Helmberger, 1972) achieves this by operating with Eq. 1.1 in terms of Laplace transforms, in which $-i\omega \rightarrow s$, and choosing the path in the complex ray parameter plane to be exactly a path of stationary phase. Chapman (1976) described how the solution in the time domain can also be obtained by the first motion approximation, which evaluates the double integral in Eq. 1.1 by the equal phase method.

Richards (1973) enumerated the advantages that accrue to the more general procedure of solving the inner integral in the frequency domain by a numerical integration along a path Γ in the complex ray parameter plane and then obtaining the time domain solution by inverse Fourier transformation. In review, these advantages are (i) that, unlike the Cagniard method, the path Γ may remain fixed for a series of distances, the only constraints being that Γ be sufficiently near all ray theory saddles and end in regions in which the integrand is exponentially small; (ii) that the method can be extended for ray paths having a turning point; (iii) that the path Γ automatically includes the non-ray theoretical effects of diffraction given by the residue contribution of ray parameter poles in the reflection-transmission coefficients; and (iv) that effects of attenuation are easily incorporated by allowing the velocity profile to be complex.

Incorporation of Attenuation

Since the solution formulae (Eqs. 1.1-1.4) are all analytical in velocity, the solution for an attenuating earth is given by analytic continuation

to a complex velocity profile defined in terms of a Q and a real velocity model (Cormier and Richards, 1976). The observation that the Q of the earth is observed to be nearly frequency independent over the broad band of seismic frequencies (10^{-2} - 10^{3} Hz) coupled with the hypothesis that the attenuation mechanism be linear leads to the relation for the complex velocity profile

$$\hat{v}(r,\omega_2) \tilde{=} v_R(r,\omega_1)\left[1 + \frac{1}{\pi Q_o(r)} \ell n \left(\frac{\omega_2}{\omega_1}\right) - \frac{i}{2Q_o(r)}\right] \tag{1.5}$$

(Liu et al., 1976), where $v_R(r,\omega_1)$ is the real velocity profile determined at the reference frequency ω_1 and $Q_o(r)$ is the Q profile. Many other representations for $\hat{v}$ can be derived by allowing for different distributions of discrete relaxation mechanisms with unequal strengths over the same frequency band.

Under several conditions the dispersive term in Eq. 1.5 can be neglected, resulting in the relation

$$\hat{v}(r) = v_R(r)\left[1 - \frac{i}{2Q_o(r)}\right] \tag{1.6}$$

The conditions under which dispersion can be neglected are that

I. calculations incorporating $\hat{v}(r)$ be over a sufficiently narrow frequency band;

II. $Q_o(r)$ be sufficiently large; and

III. the real velocity profile $v_R(r)$ be determined from data in a frequency band coincident with that of the calculation.

When either condition I or II is not met, the dispersive effect of attenuation will be manifest in a change of the shape and rise time of a propagating pulse (Futterman, 1962). Although conditions I and II affecting pulse shape may be satisfied by the pass band of most seismograph systems combined with reasonable models of the anelasticity of the upper mantle, condition III, which can bias travel times, may not. Thus knowledge of the deviation from "average" anelastic properties along a ray path may assist in applying a travel time correction when the arr ... time of that ray is used in a location determination.

A time domain study of anelasticity's effects on amplitudes, tra times, and rise times of body waves may clarify the nature of the frequency dependent anelasticity inferred from body wave spectra as reported by Lundquist (1976).

Preliminary Results

The method described by Cormier and Richards (1977) for synthesizing the seismogram of a body wave interacting with a discontinuous velocity increase has been extended to synthesize seismograms interacting with two or more such increases with any arbitrarily close spacing in depth. A test of the method was begun by synthesizing the waveform of a SH wave having a delta source time function interacting with discontinuous velocity and density increases at 420 and 670 km depth. Figure 1.1 is a reduced travel time curve for SH waves in this earth model. Initial calculations incorporated a complex velocity profile of the type given by Eq. (5) but with $Q_o(r)$ taken to be $\geq 10^5$. Later calculations will test the effect of anelasticity on waveform and apparent travel times

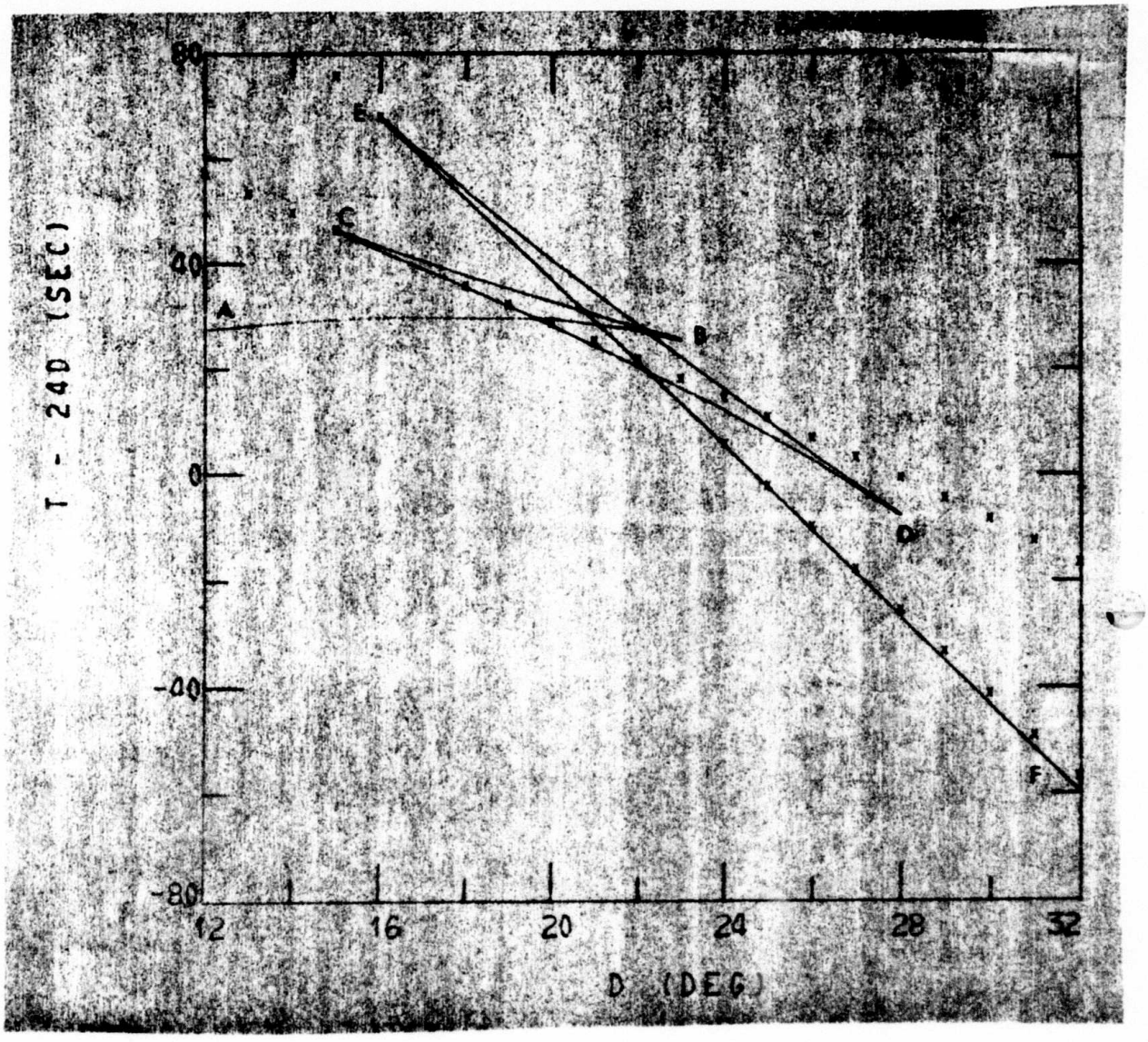

Fig. 1.1 Reduced travel time curve for SH waves in the upper mantle of earth model 1066B. Weaker arrivals (x's) at distances less that E and C are partial reflections from discontinuous velocity increases at 420 and 670 km. At distances greater than 20° the x's represent the interference head waves along these discontinuities.

with reasonable Q models of the upper mantle.

Figure 1:2 shows the synthesized SH waveforms in the distance range 30-34°. Note that the abrupt cutoff of a ray arrival at cusp D at 28° predicted by geometrical ray theory (valid at infinite frequency) becomes (at finite frequency) a gradual decay in amplitude at distances greater than D . Note also that the interference head waves associated with the 420 and 670 km discontinuities persist for long distances at which the simply transmitted ray bottoms below both discontinuities. The amplitude of such head waves has been shown to be strongly sensitive to the anelastic properties along the underside of the velocity discontinuities (Hill, 1971).

Interference of the travel time branches results in a maximum peak-to-peak amplitude of the SH body wave near 20° (Helmberger and Engen, 1974). The amplitude growth near 20° will be diagnostic of both the elastic and anelastic properties of the earth in the depth range 300-700 km. Only a synthesis incorporating both properties as depth dependent parameters can separate their competing effects (Kennett, 1975).

Synthetics for long period SH body waves will be completed for the distance range 12°-34° for an earth model with sharp discontinuities in the upper mantle and for several attenuation mechanism models in the depth range 100-700 km. It is hoped that by comparison with observed SH waveforms in this distance range some new constraints may be obtained regarding elastic and anelastic structure in the upper mantle.

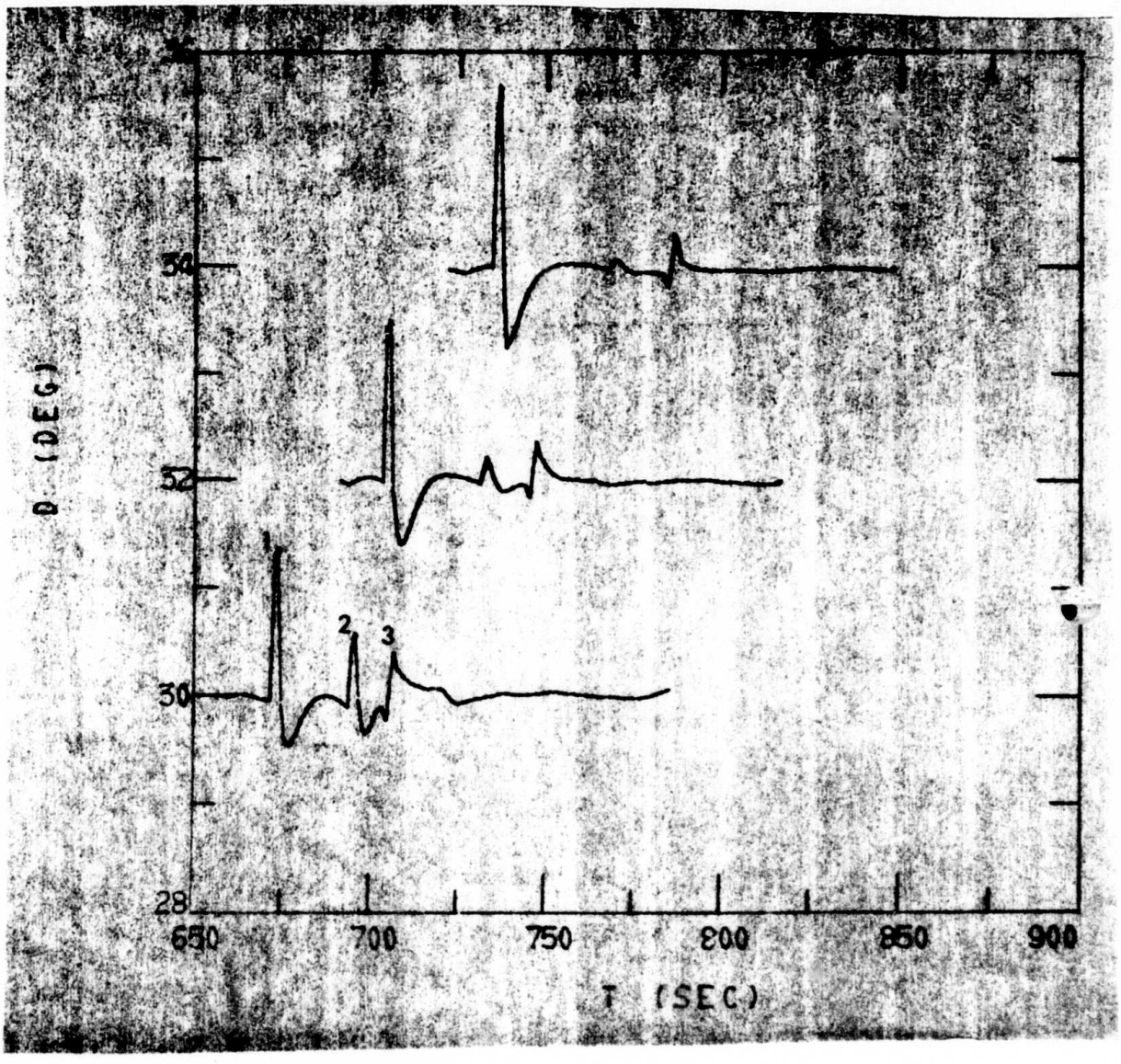

Fig. 1.2 **Response of earth model 1066B to a delta source time function in SH displacement** (surface focus) convolved with the instrument response of a 15-100 WWSSN seismograph. (1) SH wave transmitted through **670 km discontinuity plus interference head wave along that discontinuity; (2) total reflection plus diffraction from 420 km discontinuity; (3) interference head wave associated with 420 km discontinuity.**

Upper mantle with regions of intense but continuous variations in elastic properties

Introduction

By proper choice of the radial eigenfunctions that solve the potential wave equation in an inhomogeneous medium, the number of layers required to describe the medium is minimized and thereby also the number of reflection-transmission coefficients required to be evaluated in the factor f in Eq. 1.1. By allowing the layers to be inhomogeneous, in which the elastic properties vary slowly, only the coefficients associated with first-order discontinuities need to be evaluated. Langer's uniformly asymptotic approximation to the radial eigenfunctions can be used to evaluate coefficients that are valid for ray parameters corresponding to rays both near grazing and steep incidence to a discontinuity (Richards, 1976).

Suppose now, however, that the medium contained no first order discontinuities but only thin regions in which elastic properties varied rapidly, bounded by at most second-order discontinuities. Figure 1.3 compares two possible velocity distributions in the upper mantle assuming either first order discontinuities or continuous variation in elastic properties. A representation of displacement such as Eq. 1.1 can be obtained for a continuous medium in either the Cagniard or reflectivity methods by modeling the regions of rapid variation by a sequence of many thin homogeneous layers.

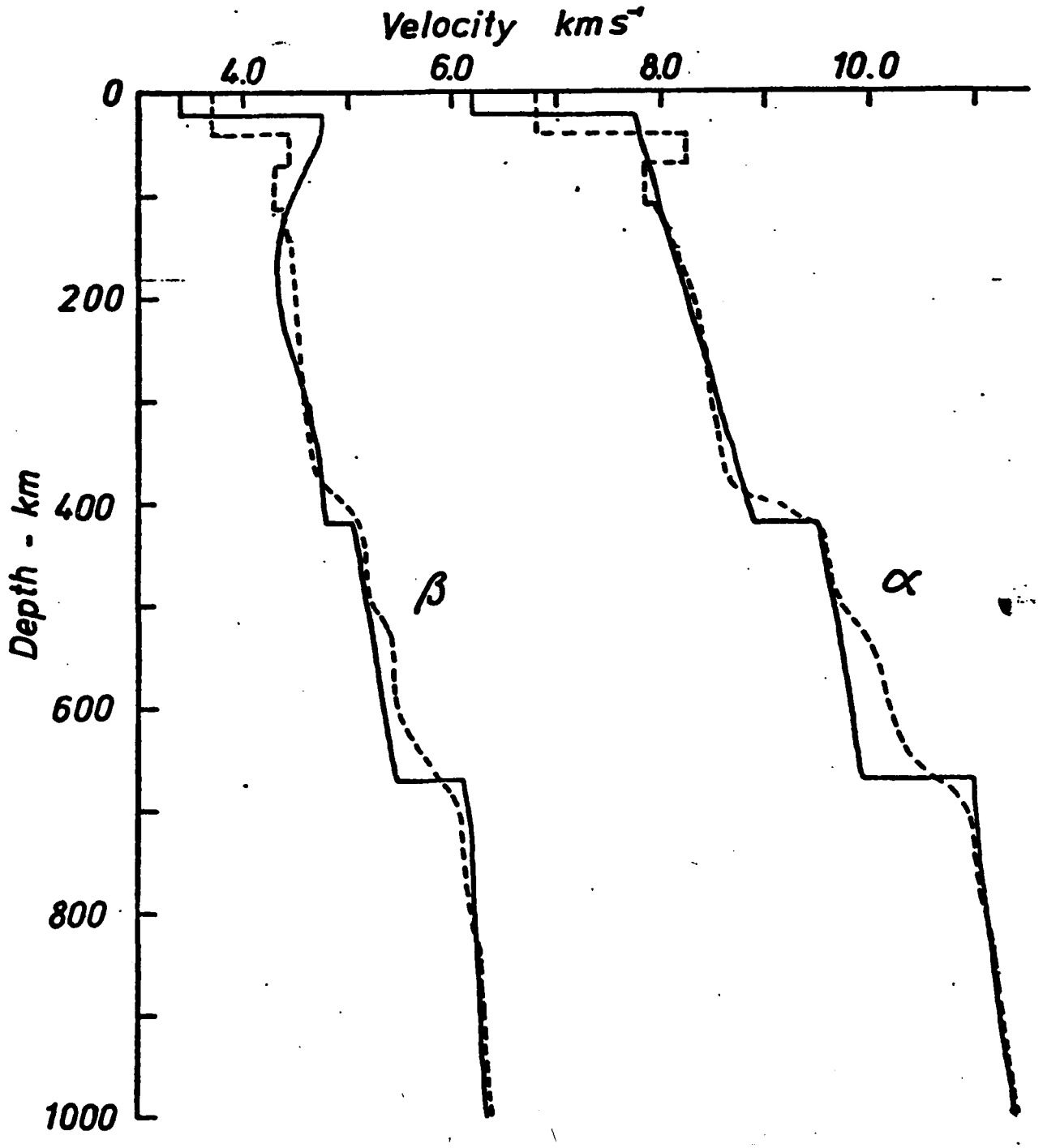

Fig. 1.3 Possible veloicty distributions in the upper mantle. Solid line - 1066B (Gilbert and Dziewonski, 1975), dashed line - SHR14 (Helmberger and Engen, 1974).

Second Order Wave Equations

To avoid a lengthy calculation for the factor f to include the many possible multiple reflections in such a stack of layers, one can seek a higher-order approximation to the radial eigenfunction. Such an approximation must be accurate at the lowest frequencies required to synthesize long period body waves and can be obtained from the second-order Helmholtz equations satisfied by P, SV, and SH potentials. These potentials are given by Richards (1974) as

$$\nabla^2 P + \frac{\rho\omega^2}{\lambda+2\mu} P + \varepsilon_P P = \frac{K_1}{\rho^{1/2}\omega^2} \frac{\partial U_r}{\partial r} + O\left(\frac{|U|}{\omega^2}\right) \tag{1.7a}$$

$$\nabla^2 V + \frac{\rho\omega}{\mu} V + \varepsilon_{SV} V = \frac{K_1}{\rho^{1/2}\omega^2} \left(0 , \frac{1}{r \sin\theta} \frac{\partial U_r}{2\phi} , \frac{1}{r} \frac{\partial U_r}{\partial\theta}\right) + O\frac{|U|}{\omega^2}\Big) \tag{1.7b}$$

$$\nabla^2 H + \frac{\rho\omega^2}{\mu} H + \varepsilon_t H = 0 \tag{1.7c}$$

for P, SV, and SH waves, respectively. (λ , μ are elastic constants, ρ density, ε_t , ε_{SV} , ε_P , K_1 functions of the density, elastic constants, and their first and second order radial derivatives, and $U = (U_r , U_\theta , U_\phi)$ is the vector displacement.)

A separation of variables allows the angular dependence of P , V , and H to be satisfied by vector surface harmonics that can be factored out of Eqs. 1.7a-1.7c, resulting in the scalar radial equations

$$\frac{d^2X}{dr^2} + \omega^2 Q_1^2 X + \varepsilon_P X = \frac{K_1 r}{\rho\omega^2} \left[\frac{d^2(X/r)}{dr^2} - \frac{B\partial Y}{r^2 \partial r}\right] + O\left(\frac{X}{\omega}\right) \tag{1.8a}$$

$$\frac{d^2Y}{dr^2} + \omega^2 Q_2\, Y + \varepsilon_{SV} Y = -\frac{K_1}{\rho\omega^2 r}\left[r\,\frac{\partial(X/r)}{\partial r} - \frac{BY}{r}\right] + O\left(\frac{Y}{\omega^2}\right) \qquad (1.8b)$$

$$\frac{d^2Z}{dr^2} + \omega^2 Q_2\, Z + \varepsilon_t\, Z = 0 \qquad (1.8c)$$

where $Q_1 = \left(\frac{1}{\alpha^2} - p^2/r^2\right)^{1/2}$

$Q_2 = \left(\frac{1}{\beta^2} - p^2/r^2\right)^{1/2}$

$B = -\omega^2 p^2$

for a P velocity function α , S velocity function β , and ray parameter p . The functions X , Y , and Z divided by r are the radial eigenfunctions of the full potentials P , V , and H , respectively.

First-Order Solutions

Within a constant of proportionality to be determined by a normalization criterion, Langer's (1951) uniform approximation to the solutions X , Y , and Z can be expressed at the lowest order in frequency as (Richards, 1976)

$$X = \left(\xi_1/Q_1\right)^{1/2} H^{(1)}_{1/3}(\omega\xi_1) \qquad (1.9a)$$

$$Y = \left(\xi_2/Q_2\right)^{1/2} H^{(1)}_{1/3}(\omega\xi_2)/\omega p \qquad (1.9b)$$

$$Z = \left(\xi_2/Q_2\right)^{1/2} H^{(1)}_{1/3}(\omega\xi_2) \qquad (1.9c)$$

where $H^{(1)}_{1/3}$ is a spherical Hankel function of order 1/3 and kind (1) for

an upgoing or (2) for a down going wave and $\xi_{1,2}$ are defined by

$$\xi_i = \int_{r_p}^{r} Q_i dr \tag{1.10}$$

In order that the coupled equations for P and V (X and Y) be dimensionally correct, the factor ωp (constant in r) must appear as shown in the solution for Y .

To first order in frequency the P and SV potentials are decoupled and the properties of the first and higher order radial derivatives of elastic moduli and density given by the factors ε_p , ε_{SV} , and ε_T do not appear in the solution. The solutions given above, however, do correctly account to first order for the effects of radial inhomogeneity near the turning point of a ray. These solutions are valid for body waves of frequency 0.01 Hz or more except in regions of severe velocity and/or density gradient in the upper mantle low velocity and transition zones.

Higher Order Solutions

Higher order uniform approximations may be determined from a perturbation solution for the functions $A(r,\omega)$ and $B(r,\omega)$ in

$$V = A(r,\omega)u + B(r,\omega)u' \tag{1.11}$$

where V symbolizes X , Y , or Z and u symbolizes a first order solution given by Eq. 1.9a, b, or c. Earlier studies (Cherry, 1950; Olver, 1974; Chapman, 1976) work with the Langer transformation of Eqs. 1.8a-c which

for a particular radial function V is of the form

$$\frac{d^2\tilde{V}}{dz^2} - [\omega^2 z - g(z,\omega)]\,\tilde{V} = 0 \qquad (1.12)$$

where $\omega g(z,\omega) = \frac{\varepsilon}{\theta'^2} + \frac{3}{4}\frac{\theta''^2}{\theta'^4} - \frac{1}{2}\frac{\theta'''}{\theta'^3}$, $z = \theta(r) = \frac{Q^2}{\theta'^2} = -(3/2\xi^{2/3})$, and $\tilde{V} = \theta'^{1/2}V$.

A perturbation solution seeks the evaluation of the functions $\tilde{A}(r,\omega)$ and $\tilde{B}(r,\omega)$ in

$$\tilde{V} = \tilde{A}(z,\omega)\ bi(\omega^{2/3}z) + \tilde{B}(z,\omega)\ bi'(\omega^{2/3}z) \qquad (1.13)$$

where bi denotes an Airy function of the first or second kind and (') a derivative with respect to z . It should be noted that the solution given by Eq. 1.13 is equivalent to that given by Eq. 1.11 after back-transforming $\tilde{V}$ to V and expressing bi in terms of Hankel functions of order 1/3 .

The evaluation of the functions $\tilde{A}$ and $\tilde{B}$ involve integrals over the variable z of integrands containing the function $\omega g(z,\omega)$. Numerical integration over z in seismic applications requires that simple functions of radius in $\omega g(z,\omega)$ such as ε be determined as complicated functions of z . If the variable of integration were changed from z to r , functions such as ε could be easily evaluated, but the functions θ' , θ'' , and θ''' resulting from the Langer transformation would be time consuming to evaluate as functions of r . Thus the alternative solution form given by Eq. 1.11 will be sought because the integrals needed to determine the coefficients of $A(r,\omega)$ and $B(r,\omega)$ in power series of

of frequency ω are integrals over radius of simple functions of radius.

In seeking such a solution, let

$$X = A(r,\omega)x + B(r,\omega)x' \tag{1.14a}$$

$$Y = \bar{A}(r,\omega)y + \bar{B}(r,\omega)y' \tag{1.14b}$$

$$Z = C(r,\omega)\bar{y} + D(r,\omega)\bar{y}' \quad , \tag{1.14c}$$

where

$$x = (\xi_1/Q_1)^{1/2} H^j_{1/3}(\omega\xi_1) \tag{1.15a}$$

$$y = (\xi_2/Q_2)^{1/2} H^j_{1/3}(\omega\xi_2)/\omega p \tag{1.15b}$$

$$\bar{y} = (\xi_2/Q_2)^{1/2} H^j_{1/3}(\omega\xi_2) \quad , \tag{1.15c}$$

$$A(r,\omega) + \sum_{n=0}^{\infty} \omega^{-2n} A_n(r) \tag{1.16a}$$

$$B(r,\omega) = \sum_{n=0}^{\infty} \omega^{-2n} B_n(r) \tag{1.16b}$$

and similarly for $\bar{A}$, $\bar{B}$, C , and D . For example, in ascending negative powers of frequency the first three terms in the solution for Z would be

$$Z = C_o(\xi_2/Q_2)^{1/2} H^j_{1/3}(\omega\xi_2) + \frac{D_1(\xi_2 Q_2)^{1/2} H^j_{2/3}(\omega\xi_2)}{\omega}$$

$$+ \frac{C_1\left[(\xi_2/Q_2)^{1/2} + D_1(\xi_2/Q_2)^{-1/2}\left(\frac{Q_2^2 - Q_2'\xi}{Q_2^2}\right)\right] H^j_{1/3}(\omega\xi_2)}{\omega^2}$$

$$+ \ . \ . \ . \ . \ . \tag{1.17}$$

To determine the coefficients A_n , B_n , etc., the solution forms of Eqs. 1.14a-c are substituted in the radial Eqs. 1.9a-c and terms in equal powers of frequency are equated.

The results for the zeroth and first higher order term for P , SV , and SH are as follows:

$$X = L_j(\xi_1/Q_1)^{1/2} H^j_{1/3}(\omega\xi_1) + \frac{L_j I_P (\xi_1/Q_1)^{1/2} H^j_{2/3}(\omega\xi_1)}{2\omega} + \ldots \quad (1.18a)$$

$$\omega pY = \bar{L}_j(\xi_2/Q_2)^{1/2} H^j_{1/3}(\omega\xi_2) + \frac{\bar{L}_j I_{SV} (\xi_2/Q_2)^{1/2} H^j_{2/3}(\omega\xi_2)}{2\omega} + \ldots \quad (1.18b)$$

$$Z = \bar{L}_j(\xi_2/Q_2)^{1/2} H^j_{1/3}(\omega\xi_2) + \frac{\bar{L}_j I_{SH} (\xi_2/Q_2)^{1/2} H^j_{2/3}(\omega\xi_2)}{2\omega} + \ldots \quad (1.18c)$$

where L_j and $\bar{L}_j$ are normalization constants for up- (j=1) or down- (j=2) going waves. The functions I_P , I_{Sv} , I_{SH} are defined by

$$I_P = \int_{r_{P_1}}^{r} \frac{[\varepsilon_P - \gamma_1 + K_1/\rho(Q_1^2 + \sigma^{jk}_{PS})]dr}{Q_1} \quad (1.19a)$$

$$I_{SV} = \int_{r_{P_2}}^{r} \frac{[\varepsilon_{SV} - \gamma_2 + K_1/\rho(p^2/r^2 + \sigma^{jk}_{SP})]dr}{Q_2} \quad (1.19b)$$

$$I_{SH} = \int_{r_{P_2}}^{r} \frac{(\varepsilon t - \gamma_2)\, dr}{Q_2} \quad , \quad (1.19c)$$

where $\gamma_i = \frac{1}{2Q_i}\frac{d^2Q_i}{dr^2} - \frac{3}{4Q_i^2}\left(\frac{dQ}{dr}\right)^2 + \frac{5}{36}\left(\frac{Q_i^2}{\xi_i^2}\right) - \frac{1}{4r^2}$,

and the coupling coefficients σ^{jk}_{PS} , σ^{jk}_{SP} by

$$\sigma_{PS}^{jk} = \frac{\bar{A}_k}{A_j} \left(\frac{\xi_2 Q_2 Q_1}{\xi_1} \right)^{1/2} \frac{p}{r} \frac{H_{2/3}^{k}(\omega\xi_2)}{H_{1/3}^{j}(\omega\xi_1)}$$

and

$$\sigma_{SP}^{jk} = \frac{A_k}{\bar{A}_j} \left(\frac{\xi_1 Q_2 Q_1}{\xi_2} \right)^{1/2} \frac{p}{r} \frac{H_{2/3}^{k}(\omega\xi_1)}{H_{1/3}^{j}(\omega\xi_2)}$$

The coupling coefficients as they appear in the second order term for P and SV waves represent singly converted waves that ususally arrive at times and distances removed from those of a wave directly transmitted through a region of anomalously large gradient when the region is much deeper than either the source or receiver.

To accurately calculate the third order term for the P and SV potential solutions, the corrections $O(X/\omega)$ and $O(Y/\omega^2)$ noted in Eqs. 7a-b must be found. The results of calculating the next higher order term for SH indicate that this term is of order $I_{SH}^2 \bar{y}/\omega^2$. Thus we may predict that the third order terms for P and SV are of order $I_P^2 x/\omega^2$ and $I_{SV}^2 y/\omega^2$. The third order P and SV terms will also involve coupling coefficients appearing in double integrals of the form

$$\int_{r_p}^{r} g(r)\, \sigma_{PS}^{jk} \left[\int_{r_p}^{r'} f(r')\, \sigma_{PS}^{jk}\, dr' \right] dr$$

Physically these double integrals involving coupling coefficients represent waves that travel essentially as converted waves in regions of intense gradient, converting back to the original wave type after leaving the region on their way towards the receiver.

Displacement

The higher order terms in the Langer approximation may be applied to determining the reflection-transmission coefficients of elastic waves incident on a radial discontinuity of first, second, or third order in elastic moduli or density. Thus fewer but more complicated factors need to be evaluated in the determination of the factor f in Eq. 1.1.

Let us now instead consider the problem of wave propagation in a hypothetical medium in which the elastic moduli and density are everywhere analytic in depth but exhibit intense gradients in certain depth ranges. Although elastic moduli and density and their first and higher order derivatives may rapidly change in certain zones in the earth, let us assume that they nevertheless change continuously. The advantages given by this assumption are (1) that the representation for potential or displacement at the surface as an integral over ray parameter does not require reflection-transmission coefficients to appear in the integrand, and (2) that the WKBJ approximation to the radial eigenfunctions may be substituted because these functions need only to be evaluated at the source and receiver radius far from a turning point.

Using the equations relating displacement $\underline{U}$ and potential

$$\underline{U} = \mu^{1/2}\left(0,0,-\frac{\partial H}{\partial \Delta}\right) \qquad \text{for SH waves and} \tag{1.20}$$

$$\underline{U} = \frac{1}{f_1}\,\text{grad}\left(\frac{f_1}{\rho^{1/2}}\,\frac{P}{r}\right) + \frac{1}{f_2}\,\text{curl curl}\left(\frac{rf_2}{\rho^{1/2}}\,\frac{V}{r}\,,\,0\,,\,0\right)$$

$$-\frac{K_1}{\rho\omega^2}\,(U_r\,,\,0\,,\,0) + \frac{K_2}{\rho\omega^2}\,\underline{U} \tag{1.21}$$

for P and SV waves, a representation for the Fourier-transformed displacement as an integral over ray parameter may be obtained as outlined by Richards (1973). Including now the first higher order term in the potentials results in a displacement representation for a source at the receiver radius and a ray departing downwards from the source:

$$U_r(r,\Delta) = \omega^{1/2} L_P \int_\Gamma p^{1/2} \left(1 + \frac{e^{i\pi/2} I_P}{\omega}\right) e^{i\omega J(r,p)} \, dp \qquad (1.22a)$$

$$U_\theta(r,\Delta) = \omega^{1/2} L_{SV} \int_\Gamma p^{1/2} \left(1 + \frac{e^{i\pi/2} I_{SV}}{\omega}\right) e^{i\omega \bar{J}(r,p)} \, dp \qquad (1.22b)$$

$$U_\phi(r,\Delta) = \omega^{1/2} L_{SH} \int_\Gamma p^{1/2} \left(1 + \frac{e^{i\pi/2} I_{SH}}{\omega}\right) e^{i\omega \bar{J}(r,p)} \, dp \qquad (1.22c)$$

when only the radial displacement U_r of a P wave and horizontal displacement U_θ of a SV wave is calculated. The constants L_P, L_{SV}, L_{SH} are proportional to the source normalization factor and seismic moment. The phase factor J is calculated in the P velocity profile and $\bar{J}$ in the S velocity profile. Note that the $\pi/2$ phase shift of the higher order term in the integrand may be interpreted as the phase shift expected of reversed travel time branches generated by regions of intense gradient.

Summary and Conclusions

A higher order Langer approximation has been developed for the radial eigenfunction of the second order wave equations satisfied by P and S potentials. The higher order approximation allows a more exact solution to the elastic wave equations in regions of strong gradient of velocity and density, remains valid for a turning point in such regions, and

minimizes the number of radially inhomogeneous layers required to describe an earth model. Coefficients in the perturbation series solution are expressed as integrals of functions of velocity, density, and their radial derivatives over the depth coordinate rather than over the Langer transformed coordinate. The coefficients can be inexpensively evaluated to third order in frequency for SH and to second order for P and SV waves. The second order term in the approximation for P and SV waves includes the effect of single P-SV scattering by regions of strong gradient. When such regions are sufficiently far from the source and receiver, these scattered waves arrive either at distances far from the receiver or at times removed from the arrival time of the transmitted wave. Thus they may represent an important source of non-intrinsic attenuation for low frequency P and SV waves in the upper mantle.

Test calculations are now in progress using the displacement representation given by Eqs. 1.22a-c in simple models of upper mantle transition zones. Comparisons of seismograms calculated using this representation for waves interacting with a thin zone of rapidly increasing velocity and density will be made with seismograms interacting with a discontinuous velocity increase at the same depth. These comparisons and calculations will be used to clarify how, if at all, the representation given by Eqs. 1.22a-c may account for narrow as well as wide angle reflections from transition zones.

References

Chapman, C. H. (1974). The turning point of elastodynamic waves, Geophys. J. R. astr. Soc. 39, 613-621.

Chapman, C. H. (1976). A first motion alternative to geometrical ray theory, Geophys. Res. Lett. 3, 153-156.

Cherry, T.M. (1950). Uniform asymptotic formulae for functions with transition points, Trans. Am. Math. Soc. 68

Cormier, V. F. and P. G. Richards (1976). Comments on 'The damping of core waves' by Anthony Qamar and Alfredo Eisenberg, J. Geophys. Res. 81, 3066-3068.

Cormier, V. F. and P. G. Richards (1977). Full wave theory applied to a discontinuous velocity increase: the inner core boundary, J. Geophys. (in press).

Fuchs, K. and G. Müller (1971). Computation of synthetic seismograms with the reflectivity method and comparison with observations, Geophys. J. R. astr. Soc. 23, 417-433.

Futterman, W. (1962). Dispersive body waves, J. Geophys. Res. 67, 5279-5291.

Gilbert, F. and D. V. Helmberger (1972). Generalized ray theory for a layered sphere, Geophys. J. R. astr. Soc. 27, 57-80.

Gilbert, F. and A. M. Dziewonski (1975). An application of normal mode theory to the retrieval of structural parameters and source mechanisms from seismic spectra, Phil. Trans. R. Soc. Lond., Ser. A. 278, 187-269.

Helmberger, D. V. and G. R. Engen (1974). Upper mantle shear structure, J. Geophys. Res. 79, 4017-4028.

Herrmann, R.B. (1975). Focal depth determination from the signal character of long period P waves, Semi-Annual Tech. Rep. No. 2, ARPA Order #1827, Seismic wave propagation and earthquake characteristics in Asia, CIRES, Univ. of Colo., Boulder, Colo.

Hill, O. P. (1971). Velocity gradients and anelasticity from crustal body wave amplitudes, J. Geophys. Res. 76, 3309-3325.

Kennett, B. L. N. (1975). The effects of attenuation on seismograms, Bull. Seism. Soc. Am. 58, 179-214.

Liu, H., D. L. Anderson and H. Kanamori (1976). Seismic wave absorption and dissipation calculated from a spectrum of relaxation mechanisms (abstract), Trans. Am. Geophys. Union 57, 593.

Lundquist, G. (1976). Spectral classification of Asian seismic events, Semi-Annual Tech. Rep. No. 2, ARPA Order 3291, Seismic wave propagation and earthquake characteristics in Asia, CIRES, Univ. of Colo., Boulder, Colo.

Olver, F. J. W. (1974). Asymptotics and Special Functions, Academic Press, N. Y.

Richards, P. G. (1973). Calculation of body waves for caustics and tunnelling in core phases, Geophys. J. R. astr. Soc. 35, 243-264.

Richards, P. G. (1974). Weakly coupled potentials for high-frequency elastic waves in continuously stratified media, Bull. Seism. Soc. Am. 64, 1575-1588.

Richards, P. G. (1976). On the adequacy of plane-wave reflection-transmission coefficients in the analysis of seismic body waves, Bull. Seism. Soc. Am. 66, 701-718.

2. THE FREQUENCY DEPENDENCE OF Q

Gary M. Lundquist

Introduction.

Energy absorption in the Earth is generally measured in terms of the seismic quality factor, Q^{-1}, which is defined as the fraction of energy dissipated per wavelength: $Q^{-1} = \frac{1}{2\pi} \frac{\Delta E}{E}$. Since Q^{-1} is defined on a per cycle basis, then a constant Q^{-1} implies increasing attenuation with frequency for a given length of path. In particular, anelastic attenuation is low at low frequencies ($f < 0.1$ Hz), amounting to a few percent at most over teleseismic path lengths. Mapping Q^{-1} as a function of frequency at those wavelengths requires a method with high resolution. On the other hand, anelastic attenuation for $f > 1$ Hz may reduce wave amplitudes by several orders of magnitude, so that a low resolution technique may be used to observe $Q^{-1}(f)$.

The functional dependency of Q^{-1} on frequency has been the subject of many recent papers with two basically different thrusts. The first group presents observational evidence on Q^{-1} and concludes that Q^{-1} is independent of frequency over the period range from about 1 hour to 1 sec. This literature has been concisely reviewed by Anderson and Hart (1977), and includes data from free oscillations, surface waves, and body waves with emphasis on multiple ScS paths. Most of the accurate determinations of Q^{-1} structure or average Q^{-1} over teleseismic paths are done for waves with periods greater than 5 sec, which is also a period range of small attenuation and therefore low resolution.

A second class of papers has examined the physical dissipation mechanisms which could be responsible for anelastic attenuation. These papers were

thoroughly reviewed by Jackson and Anderson (1970), who find a marked frequency dependence for Q^{-1} associated with each individual mechanism. One of the more likely mechanisms for anelastic attenuation is grain-boundary relaxation (Solomon, 1971; Anderson and Hart, 1977), which may be modelled as a relaxation process in a standard linear elastic solid (Mason, 1958). This model predicts Q^{-1} to behave as ω for low frequencies and as ω^{-1} for high frequencies relative to the "relaxation frequency" at which absorption is a maximum. Of course, grain sizes, existence and viscosity of melt phases, and varying activation energies will lead to a range of relaxation times and therefore, a page of absorption peaks, yielding a weaker frequency dependence than would be expected from a single mechanism.

Liu et al. (1976) chose a specific distribution of relaxation times in a standard linear elastic solid which gave them a frequency independent Q^{-1} over a frequency band wider than the band of observation. Their model may be visualized as an absorption spectrum with a finite bandwidth and ω and ω^{-1} decays at lower and higher frequencies respectively. The existence of a low frequency cutoff is required for such a model, or the real part of the index of refraction would be unbounded at zero frequency (Futterman, 1962), but the position of the cutoff is not determined either by Futterman's theory or by Liu et al. In the absence of evidence to the contrary, the low frequency cutoff was placed beyond the range of observation at 10^{-4} Hz. Again, no presently available technique has sufficient resolution to resolve the existence of this cutoff, much less its position in frequency.

Anderson and Hart (1977) estimate the total bandwidth of the absorption spectrum by using other theories to estimate the total velocity dispersion, which is a required consequence of any constant Q^{-1} model (Newlands, 1954). That is, if the difference in phase velocity at the low and high frequency

cutoffs can be independently estimated, then the bandwidth is predicted by the model of Liu et al. Anderson and Hart estimate a 15 to 20% change in velocity, which corresponds under certain assumptions, to a bandwidth of 3-6 decades. If the low frequency cutoff is at 10^{-4} Hz, then five decades gives a high frequency cutoff at 10 Hz, which is used by Liu et al. (1976). A high frequency cutoff is required by causality (Lamb, 1962) but is not uniquely determined either by causality or by Anderson and Hart. The object of this report is to present evidence for a high frequency cutoff within the passband of WWSSN seismographs.

The present study of anelastic attenuation arose out of a study of body-wave seismic source spectra. The standard correction for the Earth's attenuation filter is (Ben Menshem et al., 1966)

$$G(x)\exp(\pi f\ T/Q_E) = G(x)\exp(\pi f t^*)$$

where $G(x)$ is the frequency independent geometric attenuation. Evaluation of the travel time, T, and the average or "effective" Q^{-1}, requires both elastic and anelastic Earth models. Seismic velocities are well constrained, but Q^{-1} models are still in a state of flux.

Of the models available, two California Institute of Technology Q^{-1} models were tested on spectra from several central Asian crustal earthquakes. CIT 208 was derived from short-period body waves (Julian, personal communication), and for shallow events could be represented by a distance independent $t_\alpha^* \simeq 0.42$. CIT 11 CS2 - QM, on the other hand, was determined from surface wave data (Anderson, 1967) and could be represented by $t_\alpha^* \simeq 1.0$. Of course there is no explicit frequency dependence in either model.

The discrepancy in t^*_α could be interpretted either as an error in one model or as evidence that t^* (or Q^{-1}) is frequency dependent. The first model gave intuitively acceptable corrections to the body wave spectra; while the second model so overcorrected the high frequencies that spectral content at the peak of the short-period WWSSN seismometer response would have to be discarded as noise (see Figure 2.3). Though the first model gave usable spectra, the published literature (Carpenter and Flynn, 1965; Langsten and Helmberger, 1975) suggested the second model was more correct.

The conflict was resolved by assuming that Q^{-1} decayed toward high frequency according to a standard-linear-elastic-solid model. By assuming spectral shape, and in particular by requiring the high frequencies to decay as ω^{-2} or ω^{-3}, the position of the high frequency decay could be observed for the raypaths tested. At this time it is not possible to determine whether this decay is the high frequency cutoff postulated by Liu et al. (1976), or simply a window in an otherwise constant absorption spectrum.

Theoretical Background.

The theory will be briefly reviewed to emphasize the necessary model parameters. The energy of an harmonic wave may be written in terms of its initial value, $E_o(\omega)$, and a spreading factor $G(x)$, as

$$E(\omega) = G\, E_o(\omega)\, e^{2i(\kappa x - \omega t)} \qquad (2.1)$$

where $\kappa = \kappa' + i\kappa''$ is a complex wave number. Q^{-1} has already been defined as the fraction of energy dissipated per wave length, λ,

$$Q^{-1} = \frac{1}{2\pi} \frac{E(n\lambda) - E((n+1)\lambda)}{E(n\lambda)} \qquad (2.2)$$

If energy loss is small, then to first order the energy carried is given by 2.1 and

$$Q^{-1} = 1 - e^{-2\kappa''/\kappa'}$$

For small κ'' , the series expansion of the exponential gives

$$Q^{-1} = \frac{2\kappa''}{\kappa'} \tag{2.3}$$

That is, Q^{-1} may be defined in terms of the ratio of the imaginary and real parts of the wave number.

The distinction between P-wave and S-wave attenuation is obtained by writing the respective wave numbers in terms of complex velocities.

$$\kappa_\alpha^2 = \frac{\omega^2}{\alpha^2} \quad \frac{\omega^2}{1/\rho(\kappa + 4/3\mu)}$$

$$\kappa_\beta^2 = \frac{\omega^2}{\beta^2} = \frac{\omega^2}{\mu/\rho}$$

where κ and μ are complex bulk and shear moduli respectively. For the case of small attenuation, the ratio of imaginary to real parts gives

$$Q_\alpha^{-1} = \frac{\kappa'' + 4/3\mu''}{\kappa' + 4/3\mu'}$$

$$Q_\beta^{-1} = \frac{\mu''}{\mu'} \tag{2.4}$$

These definitions of Q^{-1} may be related to relaxation phenomena through the standard linear elastic solid (Mason, 1958). The model may be visualized as a

spring of stiffness, M_1 , in series with a parallel combination of dashpot (viscosity η) and spring (stiffness M_2). At high frequencies, or upon sudden application of stress, the system has an instantaneous elastic response controlled by M_1 , the unrelaxed system elastic modulus. At low frequencies, or upon application of a constant stress, the system modulus is that of the series springs

$$M_R = \frac{M_1 M_2}{M_1 + M_2}$$

The anelastic dashpot controls the frequency range over which the change in modulus takes place, and therefore the frequency band over which absorption takes place.

The stress strain relation for a linear elastic solid is (Liu et al., 1976)

$$\sigma + \tau_\sigma \dot{\sigma} = M_R(\epsilon + \tau_\epsilon \dot{\epsilon}) \tag{2.5}$$

where $\tau_\sigma = \eta(M_1 + M_2)$ is the stress relaxation time for constant strain, and $\tau_\epsilon = \eta/M_2$ is the strain relaxation time for constant stress. For a harmonic wave, $\dot{\sigma} = j\omega\sigma$ and $\dot{\epsilon} = j\omega\epsilon$ so that

$$\sigma(1 + j\omega\tau_\sigma) = M_R\, \epsilon(1 + j\omega\tau_\epsilon) \tag{2.6}$$

Thus the complex modulus is

$$\frac{\sigma}{\epsilon} = M = M_R\left(\frac{1 + j\omega\tau_\epsilon}{1 + j\omega\tau_\sigma}\right) \tag{2.7}$$

Finally, Q^{-1} is the ratio of imaginary part to real part.

$$Q^{-1} = C(M_1 , M_2) \left[\frac{\omega\tau}{1 + \omega^2\tau^2} \right] \tag{2.8}$$

where $\tau = \sqrt{\tau_\sigma \tau_\varepsilon}$ is the average system relaxation time, and where $C(M_1 , M_2)$ is a constant depending upon the elastic moduli of the system. In 2.7, all of the frequency dependent behavior is isolated inside the square brackets. That factor, which shall be referred to as $R_1(\omega)$ is a peaked function with ω and ω^{-1} behavior at low and high frequencies, respectively.

These results were extended to a spectrum of relaxations by Liu et al. (1976). They assumed a linear relation between τ_σ and τ_ε of the form $1 - \tau_\sigma/\tau_\varepsilon = C<<1$ where C is a constant. Then, the distribution, say of τ_ε , completely specifies the behavior of the medium. Liu et al. chose the distribution function to be

$$D(\tau_\varepsilon) = \begin{cases} 1/\tau_\varepsilon , & \tau_1 > \tau_\varepsilon > \tau_2 \\ 0 , & \tau_\varepsilon \geq \tau_1 \; ; \; \tau_\varepsilon \leq \tau_2 \end{cases} \tag{2.9}$$

where τ_1 and τ_2 were placed outside the frequency band of observation. When these assumptions were put into the Boltzman aftereffect equation and integrated, Q^{-1} was found to have the form

$$Q^{-1} = C \left[\tan^{-1} \frac{\omega(\tau_1 - \tau_2)}{1 + \omega^2 \tau_1 \tau_2} \right] \tag{2.10}$$

Again, C is a constant, and the frequency dependence has been isolated in the square brackets. This function, which shall be referred to as $R_2(\omega)$, also has ω and ω^{-1} behaviors, but about a constant Q^{-1} between τ_1 and τ_2.

The Model.

The estimation of high-frequency body-wave spectra is critically dependent upon the anelastic attenuation model. In this section, a modulation technique will be developed which superimposes a frequency dependence upon an otherwise frequency independent Q^{-1} model.

From equations 2.1 and 2.3, the amplitude of a propagating stress wave in a viscoelastic medium damps according to

$$A_o e^{-\kappa'' x} e^{i(\kappa' x - \omega t)} = A_o e^{-\frac{\omega x}{2Qc}} e^{i(\kappa' x - \omega t)} \quad (2.11)$$

where A_o is an initial value, x is distance along the raypath and c is the phase velocity. Since Q^{-1} is a per cycle characterization of absorption, it is convenient to integrate the attenuation over the raypath (Carpenter, 1967)

$$\exp\left(-\omega \int \frac{dx}{2cQ(x)}\right) = \exp\left(-\frac{\omega T}{2Q_E}\right) \quad (2.12)$$

The numerical integration requires a velocity model to obtain the travel time, T, and a Q^{-1} model to obtain the effective or average Q^{-1}, Q_E^{-1}. The ratio T/Q_E will be noted as t^* in the following discussion with subscript α or β for P or S-wave values, respectively.

The modulation proposed here will be applied to the attenuation exponent in 2.6. Three simple assumptions were made: (a) t^* is a constant as a function of epicentral distance and may be represented by $t^*_\alpha = 1.0$ and $t^*_\beta = 4.0$ for crustal earthquakes. (b) The base t^* are functions of depth only. This is equivalent to assuming radially symmetric elastic and anelastic Earth models. (c) The frequency dependence of Q, should one be discovered, has a multiplicative separability from the depth dependence. That is,

$$t^*(z, f) = t^*(z)\, R_2(f) \tag{2.13}$$

where z is hypocentral depth. This last assumption preserves the simplicity of the anelastic attenuation correction represented by equation 2.12. Otherwise a separate correction would have to be computed for each frequency at each distance. The modulation, $R_2(f)$, will be taken from equation 2.10.

The modulation, $R_1(f)$, defined by 2.8 has been tested but was not as successful as $R_2(f)$. $R_2(f)$ models only a single peak. If the right-hand side of the function is used to model the decay from a spectrum of peaks the decay is too fast for any reasonable distribution of relaxation times.

The relative sizes of Q_α^{-1} and Q_β^{-1} may be derived from equation 2.4 and Poisson's ratio, σ. Note that both P and S waves are attenuated by shear loss mechanisms ($\mu'' \neq 0$), but P-waves suffer additional attenuation from bulk losses whenever $k'' \neq 0$. Bulk losses are generally neglected (Anderson and Hart, 1977), and setting $k'' = 0$ in 2.4 gives

$$\frac{Q_\beta^{-1}}{Q_\alpha^{-1}} = \frac{3}{4}\left(\frac{\alpha}{\beta}\right)^2 \qquad (2.14)$$

For a Poisson condition, $\sigma = 0.25$ and $Q_\beta^{-1}/Q_\alpha^{-1} = 2.25$.

The relative sizes of t_α^* and t_β^* depend again upon Poisson's ratio. If σ is assumed constant along the raypath and $k'' = 0$, then P and S waves follow exactly the same path (Carpenter, 1965) so that $\alpha T_\alpha = \beta T_\beta$ and

$$\frac{t_\beta^*}{t_\alpha^*} = \frac{3}{4}\frac{\alpha^3}{\beta^3} \qquad (2.15)$$

For mantle velocities, $t_\beta^*/t_\alpha^* = 4.16 \rightarrow 4.84$.

An important feature of t_β^*/t_α^* is that this ratio of ratios cannot increase as a function of frequency. If all losses are in shear, then t_β^*/t_α^* is a constant because Q_α^{-1} , Q_β^{-1} , T_α and T_β all change in constant proportion. If a bulk loss operates over some frequency range, then t_α^* can only increase, because Q_α^{-1} increases much faster than the slight decrease in T_α due to body-wave dispersion.

The absolute values of Q^{-1} and t^* are more difficult to determine. The basic model analysis reported in this paper used $t_\alpha^* = 1.0$, following Carpenter and Flynn (1965) and $t_\beta^* = 4.0$ (Helmberger, 1973). The recent Q^{-1} models of Anderson and Hart (1977) support a distance independent $t_\alpha^* = 1.0$, but suggest $t_\beta^* > 4.0$ with a more distinct dependence on distance. $t_\beta^*/t_\alpha^* = 4.0$ will be understood as a minimum value for that ratio.

Figure 2.1 shows the modulation of the total anelastic attenuation correction according to the distribution proposed by Liu et al. (1976) in equations 2.9 and 2.10. The curves marked "unmodulated" give the correction defined by equation 2.12 for a frequency independent t^* (i.e., frequency independent Q^{-1}). The other curves result from modulation by $R_2(\omega)$ (equation 2.10) where τ_1 = 2000 sec, and τ_1 is as labelled.

t^* will depend upon hypocentral depth, since earthquakes may occur below most of the highly attenuating upper mantle. Many authors (Solomon, 1971; Anderson and Hart, 1977) point out that the anelastic attenuation is dominated by the asthenosphere. An extreme case was suggested by Helmberger (1973), who modelled a 50 km thick asthenosphere in which $Q_\alpha = 50$, surrounded by a high Q (2000) mantle and crust. Burdick and Helmberger (1974) suggest $t^*_\alpha = .55$ and $t^*_\beta = 2.2$ for hypocentral depths of about 600 km. The new Q^{-1} models of Anderson and Hart (1977) suggest a much smaller change, amounting to only 30% at 600 km. For the deep earthquake reported in this paper, t^*_α was set at 0.6, and $t^*_\beta = 2.4$.

The anelastic attenuation correction curves appropriate for hypocentral depth of 600 km are shown in Figure 2.2, with the modulations by equation 2.10. The change in the relaxation parameter, τ_2, will be a subject of the next section. For now, note that the reduction in predicted attenuation reduces the resolution of the modulation technique modelled here.

The model proposed here arises out of physical considerations of absorption, but it also meets a consideration of energy conservation. Specifically, conservation of energy requires an amplitude spectrum to decay at least as fast as $\omega^{-3/2}$ as $\omega \to \infty$. But the exponential corrections implied by the unmodulated curves of Figures 2.1 and 2.2 will raise the observed spectral

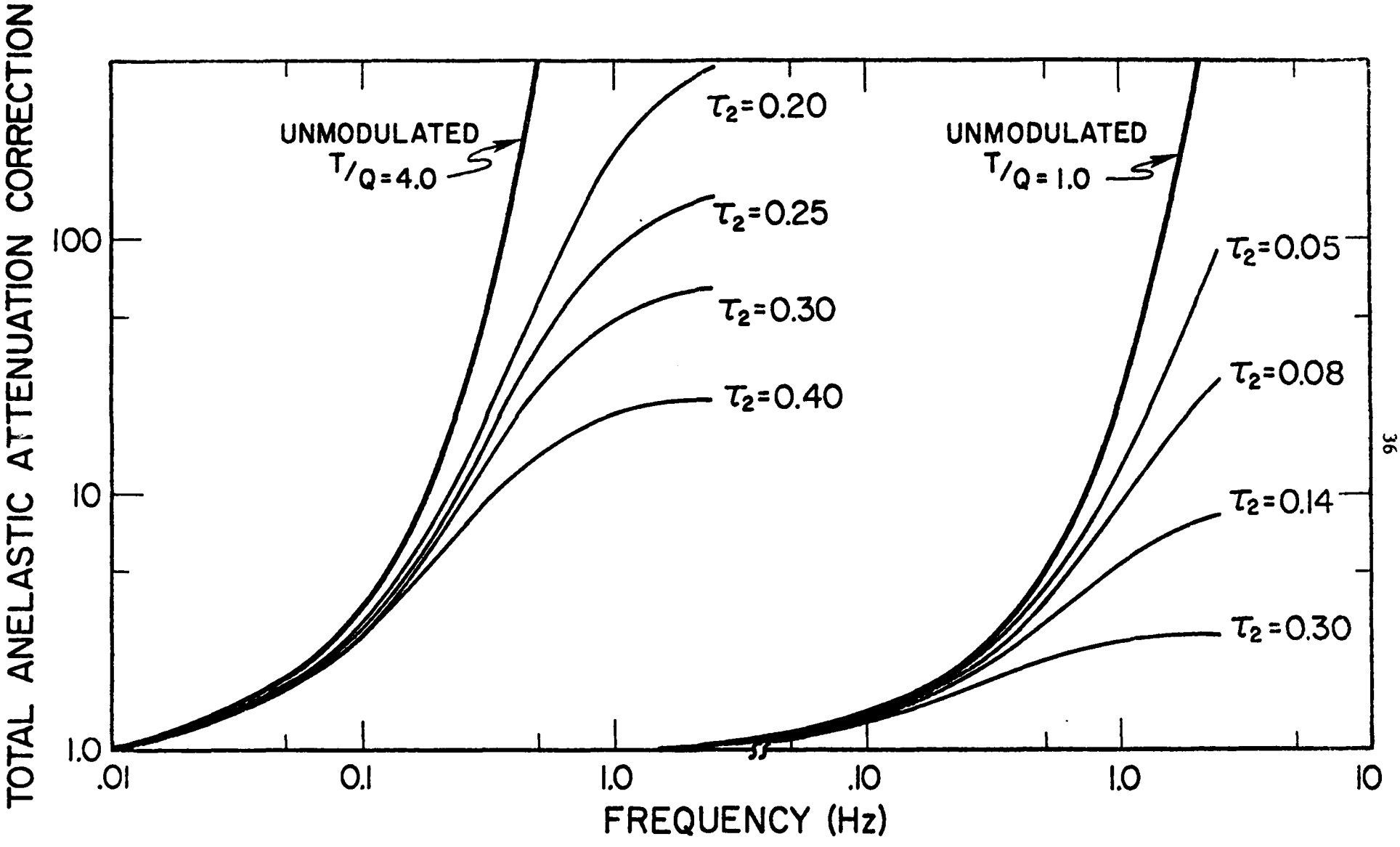

Figure 2.1: Total anelastic attenuation correction vs. frequency for crustal earthquakes. The modulated curves are based upon the model of Liu et al. (1976).

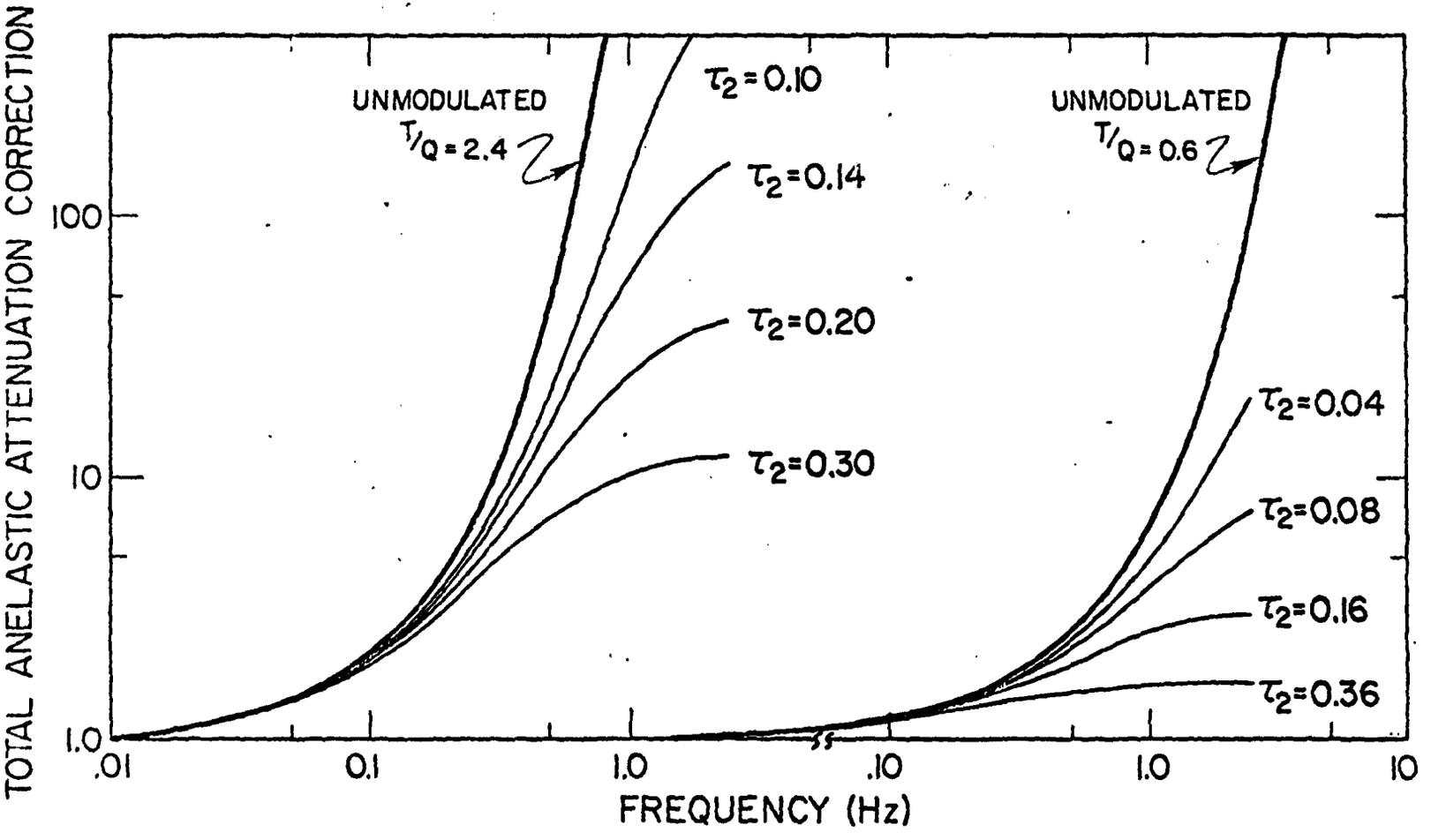

Figure 2.2: Total anelastic attenuation correction vs. frequency for deep earthquakes. The modulated curves are based upon the model of Liu et al. (1976).

decay slopes by ever increasing amounts. That is, for the unmodulated curves to be appropriate, the uncorrected station spectra must decay at a rate faster than exponential, and such a decay is not observed.

The modulation proposed will thus be interpreted and used as a decay slope modification. A characteristic of each modulated curve is that an inflection point exists beyond which the curve is concave down rather than concave up. In the limit of high frequency, each curve approaches a constant as a function of frequency, suggesting that all frequencies in that range are attenuated by the same amount. If a station spectrum with an original decay of ω^{-3} is to be interpreted according to Archambeau's (1964) relaxation seismic-source model, for instance, then all of the frequencies in the decay slope must be corrected equally. To obtain an ω^{-2} decay slope on the same hypothetical spectrum, a slope change of ω^{+1} must be given by the correction function.

Though the expected decay slope for a given earthquake-station pair is not known, the range of slopes predicted by seismic source theory is ω^{-2} to ω^{-3}. Each of those slopes will be sought as a function of the relaxation parameter, τ_2, and the implications will be examined. That is, a spectral shape will be assumed, and Earth properties will be investigated under that hypothesis.

Data.

Twelve central Asian crustal earthquakes and a deep earthquake in each of Fiji and Brazil have been tested in this study. Examples of the results are given in Figures 2.3-2.5. Each spectrum presented is an average of eight or more stations in the distance range 30-60°. The individual spectral were estimated by the autocorrelation technique of Lundquist (1977). In each case, the uppermost spectra were corrected by a frequency independent model CIT 208,

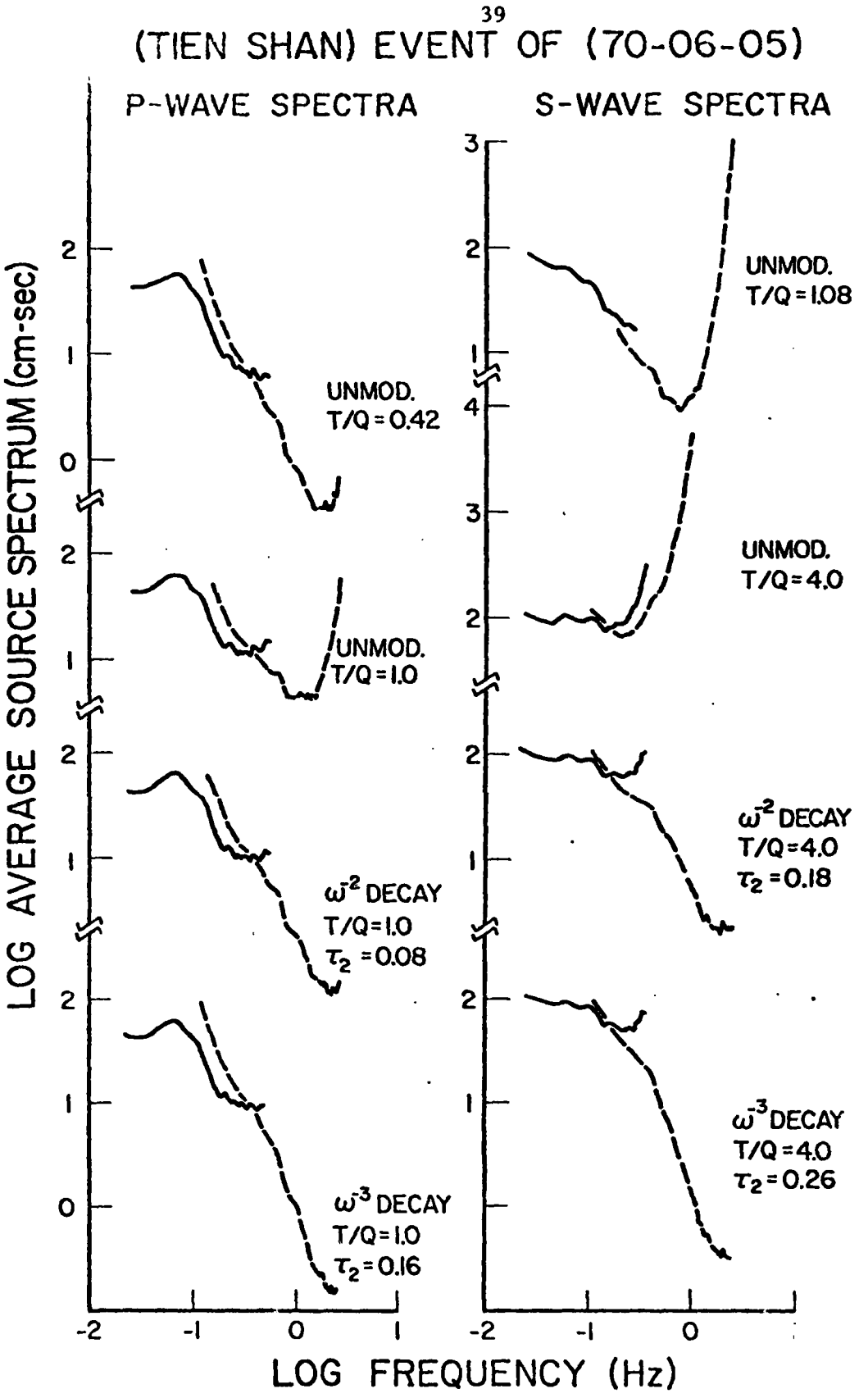

Figure 2.3: Body wave spectra for the event of 70-06-05. From top to bottom, average station spectra were corrected for anelastic attenuation by model CIT 208, CIT 11 CS2-QM with no modulation, CIT 11 CS2-QM modulated to ω^{-2} decay rate and CIT 11 CS2-QM modulated to ω^{-3} decay rate.

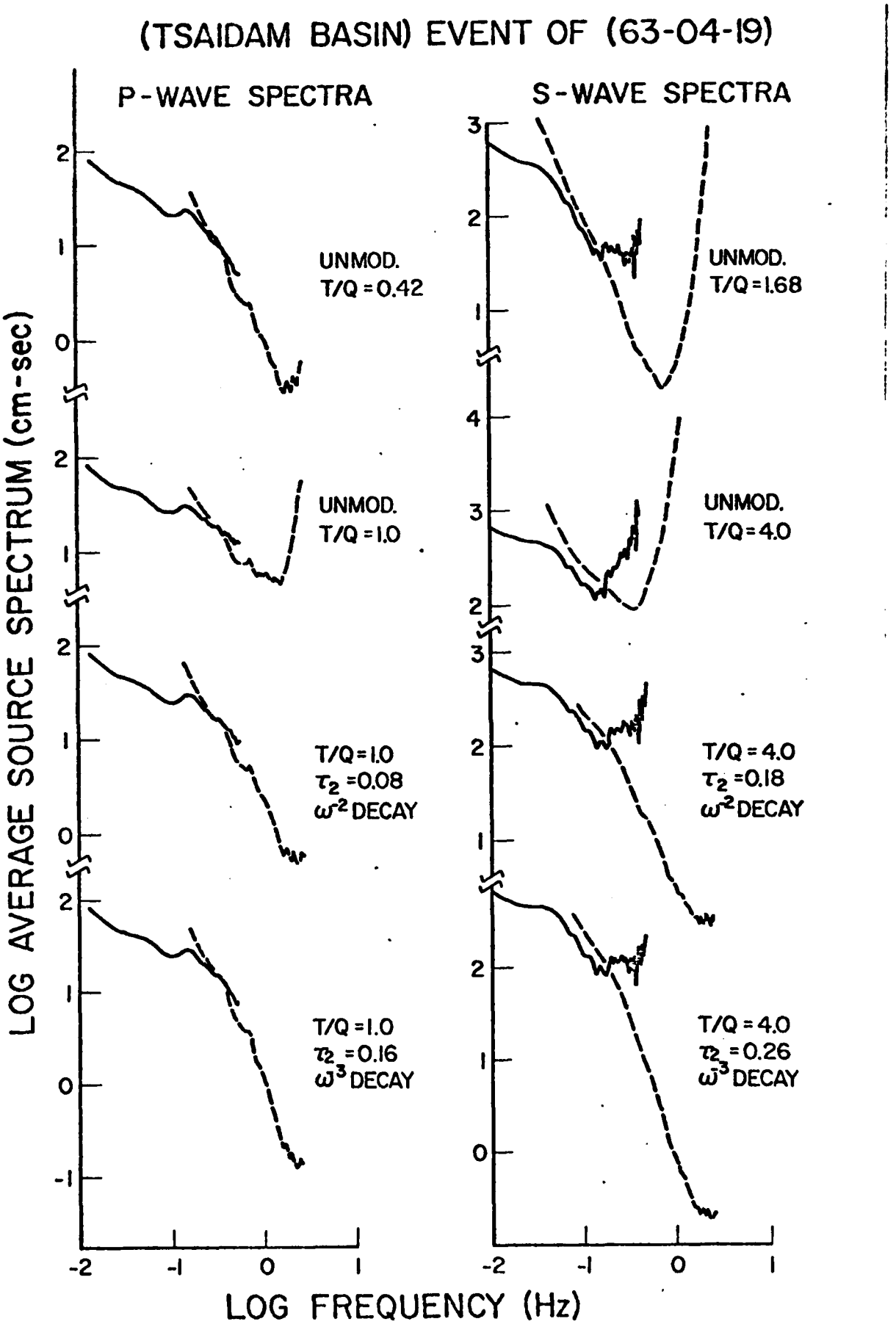

Figure 2.4: Body wave spectra for the event of 63-04-09. From top to bottom, the average station spectra were corrected for anelastic attenuation by model CIT 208, CIT 11CS2-QM with no modulation, CIT11CS2-QM modulated to ω^{-2} decay rate and CIT11CS2-QM modulated to ω^{-3} decay rate.

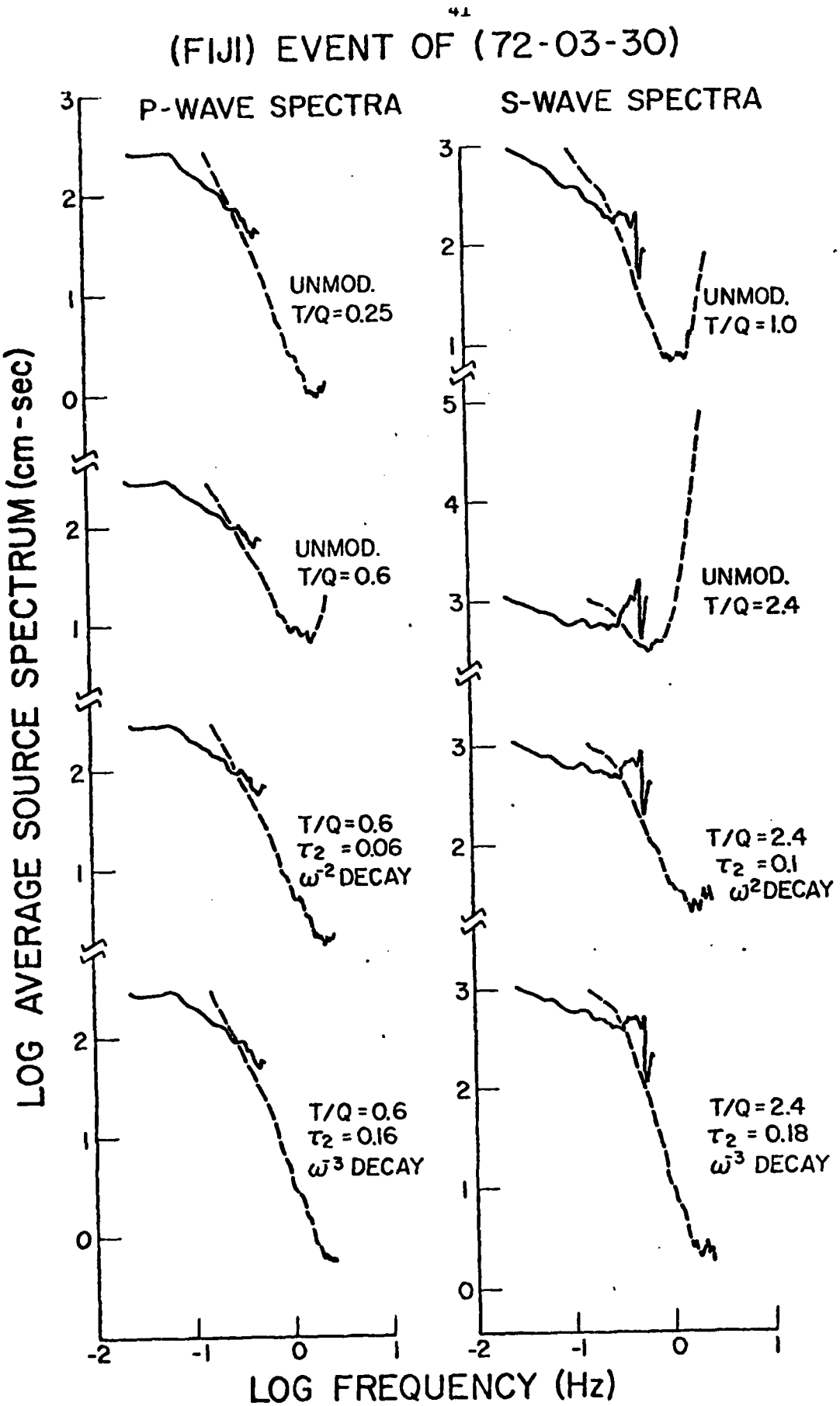

Figure 2.5: Body wave spectra for the event of 72-03-30. From top to bottom, the average spectra were corrected for anelastic attenuation by model CIT 208, CIT11CS2-QM with no modulation, CIT11CS2-QM modulated to ω^{-2} decay rate and CIT11CS2-QM modulated to ω^{-3} decay rate.

while the second set of spectra were corrected with model CIT 11 CS2-QM. The values of t^* are given on the figures and correspond to the discussion of the last section. The last two sets of spectra in each figure were selected for decay rate characteristics of ω^{-2} or ω^{-3} by specifying a frequency dependent t^* and adjusting τ_2 . The results presented are also characteristic of the other earthquakes studied.

Table 2.1 lists several important parameters, both of the attenuation correction and the resulting interpreted seismic source properties.

Discussion.

Several observations may be made from 2.3-2.5. First and most obvious are the problems with the standard corrections which nucleated this study. Though CIT 208 provides an acceptable correction for the P-wave spectra, neither of the standard models adequately accounts for the attenuation of high frequency S waves. The deviation from a constant decay rate is not a noise problem. Rather, the overcorrection results from the exponential correction function overpowering the decay rate of the station spectra. Unless the station spectrum decays faster than an exponential, the overcorrection must occur at some frequency, whether noise is present or not.

As mentioned in the last section, any fall-off less rapid than $\omega^{-3/2}$ violates conservation of energy in the limit as $\omega \to \infty$. Though these figures demonstrate that an improvement may be achieved by adjusting the base t^* values, the improvement persists only over a small frequency range. Some modulation is required to reduce the exponential rate of increase in the correction function over all positive frequencies.

A very interesting result of this experiment is the fact that the P and S wave spectra from shallow earthquakes need different modulations to achieve the same decay slope. At first glance, one might attribute the difference to

Table 2.1

Event	T/Q		Slope Adjustment	Relaxation Parameter		Seismic Moment (10^{25} dyne-cm)		Corner Freq. (Hz)		Stress Drop (Bars)	
	P	S		T_{2p}	T_{2s}	P	S	P	S	P	S
70-06-05	.42	1.68	none			10.0	3.2	.16	.08	6	1.3
Tien Shan											
42.48N	1.0	4.0	none					.08	.12	0.7	4.5
78.76E											
h = 20 km	1.0	4.0	ω^{-2}	.08	.18			.17	.24	7	36
	1.0	4.0	ω^{-3}	.16	.26			.23	.25	17	41
63-04-19	.42	1.68	none			7.0	13.0	.20	.044	8	0.9
Tsaidam	1.0	4.0	none					.095	.045	0.9	1.0
35.7N											
96.9E	1.0	4.0	ω^{-2}	.08	.18			.24	.09	14	8
h = 33 km											
	1.0	4.0	ω^{-3}	.16	.26			.28	.12	22	18
72-03-30	0.25	1.0	none			69.0	40.0	.16	.18	30	133
Fiji	0.6	2.4	none					.13	.22	15	242
25.75											
179.4E	0.6	2.4	ω^{-2}	.06	.10			.16	.22	30	242
h = 532 km											
	0.6	2.4	ω^{-3}	.16	.18			.23	.25	83	356

TABLE 1: A list of the events, anelastic attenuation model parameters and interpreted seismic source parameters.

the different t^*, but careful consideration shows that if both wave types are attenuated by the same mechanisms, then the modulation must be the same.

Figures 2.6 and 2.7 show the $t^*(f)$ for the two decay slopes tested, and both figures support the same conclusions for shallow earthquakes: (a) Either the high frequency cutoff or a window in the absorption spectrum may be resolved for both P and S waves. (b) The P waves are attenuated to higher frequencies than are S waves. Since both wave types suffer shear losses in constant proportion, the additional attenuation of P waves must result from a bulk loss.

This last possibility was discussed under the Theory section. The ratio t^*_β/t^*_α must either be constant as a function of frequency or decrease relative to a frequency range over which the imaginary bulk modulus is zero. If t^*_β/t^*_α decreases by a factor of $\delta > 0$ as a function of frequency, then equation 2.4 gives

$$\frac{k''}{\mu''} = \frac{4}{3}(\delta - 1) \qquad (2.16)$$

Under the assumptions of this model and the assumption that P and S spectra should have the same decay slope, the only conclusion is that bulk-loss mechanism operates over a narrow frequency band within the window in the S-wave absorption spectrum.

The difference between modulations required for P and S-wave spectra from deep earthquakes is not as great as the same difference for shallow earthquakes. This could result from either the low resolution, especially of P-waves, or from the limited sample of deep earthquakes tested. But the result may also be interpreted in terms of Earth properties. Suppose for a moment that the bulk loss mechanism operates only in the asthenosphere, while

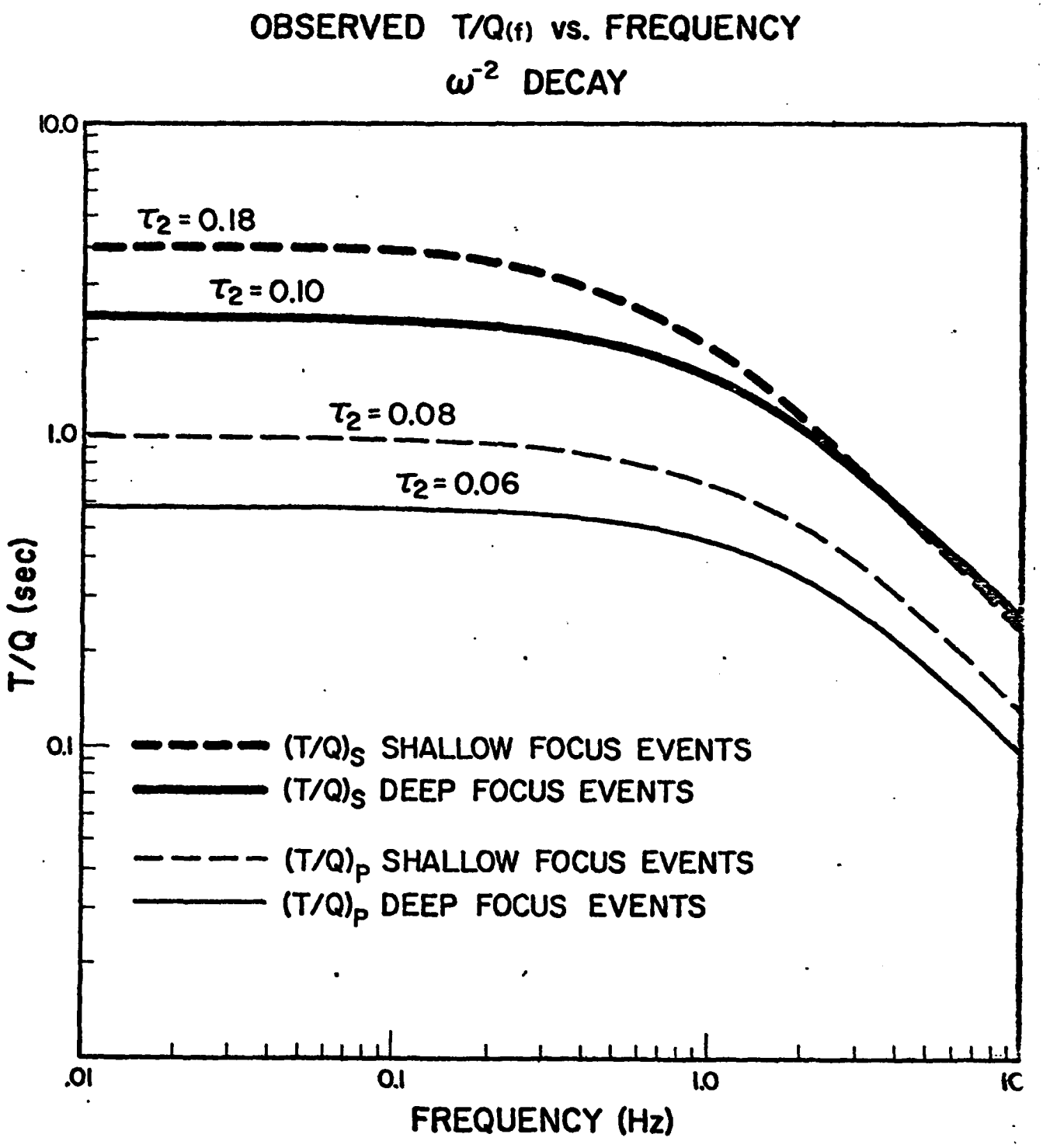

Figure 2.6: Observed t^* vs. frequency. The values of τ_2 correspond to Figures 2.3-2.5 for a high frequency spectral decay slope of ω^{-2}.

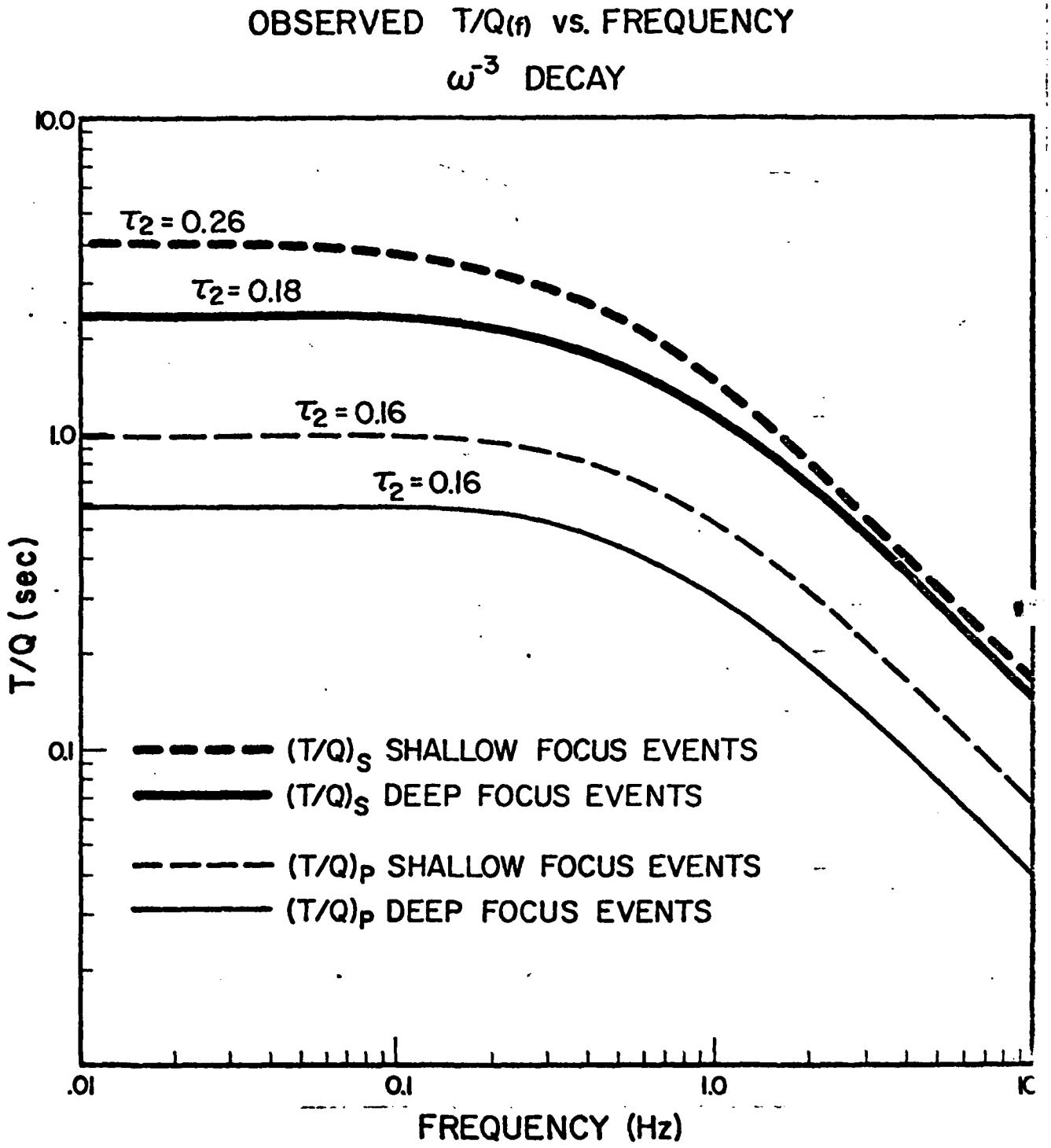

Figure 2.7: Observed t^* vs. frequency. The values of τ_2 correspond to Figures 2.3-2.5 for a high frequency spectral decay slope of ω^{-3}.

shear loss mechanism operate throughout the mantle. Then the change in path from shallow focus to deep focus must affect the P and S-wave absorption spectra differently.

In Figures 2.6 and 2.7, the P-wave absorption spectrum appears to be reduced by a constant factor as through approximately half as much attenuation were seen by the deep events as by the shallow. The reduction in the effective amplitude of k'' would also reduce the difference between P and S-wave absorption spectra, a result which is also observed in the figures.

The interpretation of the modulation change for S waves as a function of hypocentral depth is not clear, and further study will be required before this writer will forward an hypothesis. It is likely that the relaxation frequencies operating in the asthenosphere are not exactly those operating in the rest of the mantle. Though the modulation technique reported here, some information may be obtained in the location of a window or high frequency cutoff, but the simple characteristic of spectral decay does not give enough resolution to permit detailed inversion for the spectrum of relaxation frequencies.

A bulk loss mechanism which might operate over seismic frequencies was examined by Vaisnys (1968). He argues that a medium composed of a solid in equilibrium with its own melt may suffer additional phase change under compressive stress. If the stress is harmonic, the amount of phase change would vary with frequency, being peaked about $\omega = 1/\tau$, where τ is a characteristic rate of the phase change. Essentially, the medium would tend to freeze during one half of the stress cycle, then thaw during the other half cycle. Since more energy is required to order a lattice than to disorder a lattice, the effect would be a slightly greater fraction of melt after the

wave has passed. Since this mechanism requires pressure changes, it would attenuate only P waves; and, since the mechanism requires a partial melt, it would operate primarily in the asthenosphere.

The Vaisnys bulk loss mechanism was probably observed by Spetzler and Anderson (1968). They observed attenuation as a function of temperature in an ice-brine mixture and found a marked decrease in Q_α for temperatures within 3% of melting temperature. The loss mechanism is definitely related to the melting temperature, T_m, since Q_α in the near vicinity of T_m was lower than Q_α for either higher or lower temperatures.

As a side note, the Brune model (1970) stress drops were calculated for the various correction models tested, and the results are given in Table 2.1. Stress drop calculated that way depends upon the cube of the observed corner frequency, so small changes in f_o can be critical to the stress drop calculation. The table itself speaks eloquently of the importance of determining the proper anelastic attenuation correction. Until such a criterion is established, stress drop computed from body-wave spectra must be interpreted in terms of the Q^{-1} model used. In particular, comparisons of stress drops calculated under different Q^{-1} models are not valid.

Conclusions.

This study has investigated the frequency dependence of Q^{-1}, or equivalently, of t^*. Evidence for such a dependence was found by examining the correction of body-wave spectra for anelastic attenuation. The model reported here was designed to observe a high-frequency cutoff or a window in an otherwise constant absorption spectrum, and such a decay in attenuation toward high frequencies was observed for both P and S waves. When the criterion for the body wave spectra is an ω^{-3} decay, then the spectrum of relaxations controlled by

modulus has a decay beginning about .2 Hz, while a separate dissipation mechanism operating on the bulk modulus maintains P-wave attenuation out to about .4 Hz. When the criterion is an ω^{-2} decay slope, then the same conclusions apply, but the frequencies are about .35 and .7 Hz, respectively.

The change in the required model parameters as a function of depth definitely suggest that the bulk loss mechanism is concentrated almost entirely in the asthenosphere, while the losses in shear are distributed in a complex manner throughout the mantle. Thus t_α^* and t_β^* must have different behavior as a function of depth over the critical range of requencies of the absorption window.

Finally, the value of stress drop computed from body-wave spectra was shown to be very dependent upon the Q^{-1} model used to correct those spectra for anelastic attenuation.

References

Anderson, D.L., Latest information from seismic observations, chapter 12 in The Earth's Mantle (T.F. Gaskell, Editor), 355-470, Academic Press, 1967.

Anderson, D.L., and R.S. Hart, The Q of the Earth, preprint, 1977.

Archambeau, C.B., General theory of elastodynamic source fields, Rev. Geophys., 6, 241-288, 1968.

Ben Menahem, A., S.W. Smith, and T.L. Teng, A procedure for source studies from spectrums of long-period seismic body waves, Bull. Seism. Soc. Am., 55, 203-235, 1965.

Brune, J., Tectonic strain and the spectrum of seismic shear waves, J. Geophys. Res., 75, 4997-5009, 1970.

Burdick, L.J. and D. V. Helmberger, Time functions appropriate for deep earthquakes, Bull. Seism. Soc. Am., 64, 1419-1428, 1974.

Carpenter, E. W., Teleseismic signals calculated for underground, underwater and atonospheric explosions, Geophysics, 32, 17-32, 1967.

Carpenter, E.W. and E.A. Flynn, Attenuation of teleseismic body waves, Nature, 207, 745-746, 1965.

Futterman, W.I., Dispersive body waves, J. Geophys. Res., 13, 5279-5291, 1962.

Jackson, D.D. and D.L. Anderson, Physical mechanisms of seismic wave attenuation, Rev. Geophys. Space Phys., 8, 1-63, 1970.

Helmberger, D.V., On the structure of the low velocity zone, Geophys. J. R. Astro. Soc., 34, 251-263, 1973.

Lamb, G.L. Jr., The attenuation of waves in a dispersive medium, J. Geophys. Res., 67, 5273-5277, 1962.

Langston, C.A. and D. V. Helmberger, A procedure for modelling shallow dislocation sources, Geophys. J.,

Liu, H.P., D. L. Anderson and H. Kanamori, Velocoty dispersion due to anelasticity; implications for seismology and mantle composition, Geophys. J. R. Astro. Soc., 47, 41-58, 1976.

Lundquist, G.M., The estimation of seismogram spectra, submitted to Bull. Seism. Soc. Am., 1977.

Mason, W.P., Physical Acoustics and the Properties of Solids, D. Van Nostrand, Princeton, N.J., 1958.

Newlands, M.,

J. Acoust. Soc. Am., 26, 434-448, 1954.

Solomon, S.C., Seismic Wave Attenuation and the State of the Upper Mantle, Ph.D. Thesis, Massachusetts Institute of Technology, 1971.

Vaisnys, J.R., Propagation of acoustic waves through a system undergoing phase transformations, J. Geophys. Res., 73, 7675-7683, 1968.

3. SOURCE THEORY, STRESS ESTIMATION AND DISCRIMINATION

C.B. Archambeau, Carlos Salvado, and Jeff Stevens

Introduction.

During the first half of the current contract period considerable emphasis has been placed on the development of very general analytical and numerical models of seismic sources. To achieve the required generality we have considered combined analytical and numerical methods. Specifically we have considered Green's function representations of the field obtained by numerical computation within a relatively small zone surrounding the (generally nonlinear) source of seismic energy. This allows us to predict far field radiation from three dimensional nonlinear sources (such as earthquakes or complex explosions), whereas in the past the costs of numerical modeling could be prohibitive.

A second area of research has been the study of observed earthquakes using current (analytical) relaxation models of earthquakes. In particular we have studied events in the Pacific region using m_b-M_s data to estimate the tectonic stress drops and failure zone dimensions. In this study we hope not only to gain a better understanding of earthquake physics, but also to verify predictions of m_b-M_s behavior based on relaxation source theory in order to establish the basis for event discrimination. Further this approach delineates those regions producing "anomalous" (explosion-like) earthquakes and provides a basis for the description and understanding of such events.

The following section provides a brief description of some of the results and conclusions obtained from the study of the m_b-M_s data for a large set of events in the Pacific area. A final section describes, in some detail, the

theoretical approach used in the combined numerical-analytical modeling of seismic sources. Applications of this theory are in progress and will be discussed in later reports. Current applied work has progressed to the point where a specific source model will be generated in the near future (i.e., a three dimensional "ellipsoidal" earthquake in a non-homogeneous initial stress field).

Seismically Inferred Nonhydrostatic Stresses in the Earth's Lithosphere.

The large seismic data base consisting of measured values of body and surface wave magnitudes from world-side earthquakes, in the range m_b from 4.5 to 6.5, has been used to infer tectonic stress drops for events in the most active regions around the Pacific. The approach relies upon theoretical predictions of m_b and M_s for strike-slip, normal, and thrust earthquakes at a variety of depths, where the rupture velocity is assumed to be a fixed fraction of the local shear velocity and the ratio of the rupture width to length is also assumed to be a constant. The observed event data are classified as to type on the basis of location relative to known tectonic features. The stress drop and failure zone dimensions are then determined from the theoretical predictions for events of the corresponding type in the appropriate depth range. We find that the stress patterns inferred are highly variable spatially, with relatively small zones of high stress near 1 kbar. The location of such stress concentrations is usually within a seismic "gap" with regard to earthquakes much stronger than those used in the analysis. Estimation of stress before and after relatively large earthquakes shows that the large events initiate in the small zones of high stress, with stress levels being much lower in this region after the large event but usually with higher stress zones created near the limits of the failure zone. Large events nearly always show stress drops around 100 bars, which is much lower than the level that appears to

be required for initiation. This can be interpreted to mean that large events start within the high stress zones but that failure may be dynamically driven into zones of much lower stress, sometimes also across these low zones into other zones of high stress. This behavior results in a low average stress drop and the appearance of a multiple event.

Green's Function Techniques for the Representation of Elastic Wave Fields.

Two particular applications of the Green's function representation in elastodynamic theory to numerically generated wave fields are considered. First, it is shown that the Green's function representation of a wave field in the elastic zone outside of a nonlinear source region can be used to generate an equivalent elastic source that analytically reproduces a field identifical to the numerical field in the elastic region. This analytical representation of the field can then be easily employed to predict the radiation at large distances from the source. The approach therefore allows truncation of the numerical computation after a short time and allows complex linear-nonlinear problems to be attacked with much greater accuracy and efficiency. The second application employs the Green's function representation to effect a transparent boundary for the edge of a numerical grid. In this case, an infinite space (or half space) Green's function representation is used to predict the motion of the grid points on the boundary of the grid based on the motion of the points on the surface defined by the nearest interior grid points. This approach causes the grid boundary to transmit the field without reflection of energy back into the interior of the grid system and hence can greatly reduce the necessary grid size and improve numerical accuracy. This approach can greatly enhance our ability to obtain realistic representations of complex seismic sources wherein both nonlinear and linear phenomena can be modeled in an arbitrary geometry.

General Theory. We consider the general linear elastic equation of motion*

$$\frac{\partial}{\partial t}\left(\rho \frac{\partial u_i}{\partial t}\right) = \frac{\partial}{\partial x_j}\left[C_{ijk\ell} \frac{\partial u_k}{\partial x_\ell}\right] + \rho b_i \ \ldots \qquad (3.1)$$

where the stress tensor is given by

$$T_{ij} = C_{ijk\ell}\, e_{k\ell} = C_{ijk\ell}\, u_{k,\ell} = C_{ijk\ell}\, u_{(k,\ell)}$$

where $e_{k\ell} = u_{(k,\ell)}$ is the strain with $u_{(k,\ell)}$ the symmetric part of $U_{k,\ell} = \partial U_k/\partial x_\ell$ and $C_{ijk\ell}$ is the elastic tensor with symmetry relations

$$C_{ijk\ell} = C_{jik\ell} = C_{ij\ell k} = C_{k\ell ij}$$

Both ρ and the $C_{ijk\ell}$ may be functions of the spatial coordinates but have been assumed independent of time.

We may define four vectors and four tensors which allow the equation of motion and boundary conditions for elastic problems to be expressed in the compact general form:**

---

*The general reference for much of this section is Archambeau and Minster [197#], "Dynamics in Prestressed Media with Moving Boundaries: A Continuum Theory of Failure (in press, Geophys. J. R. A. S.).

**In this discussion, Cartesian tensors were used throughout. Further, Greek letters used as indices will always run over the range 1, 2, 3, 4 while Latin letters will have the range 1, 2, 3.

$$\left.\begin{aligned} L_{\alpha\gamma}\ u_\gamma &= \rho f_\alpha \\ [\![\tau_{\alpha\beta} n_\beta]\!]_\Sigma &= 0 \end{aligned}\right\} \tag{3.2}$$

α, β and γ take on the values 1, 2, 3, 4 and the first equation in 3.2 is the equation of motion while the second equation expresses the boundary conditions to be satisfied by the field U_γ on boundary surfaces Σ. Here the standard bracket notation for the jump across a boundary is used, i.e., for any function F defined on both sides Σ_1 and Σ_2 of a surface Σ, then $[\![F]\!]_\Sigma = F(\Sigma_1) - F(\Sigma_2)$ where $F(\Sigma_1)$ means F evaluated on Σ as approached from side 1 and similarly for $F(\Sigma_2)$.

Here the operator $L_{\alpha\gamma}$ in 3.2 is defined as

$$L_{\alpha\gamma} \equiv \frac{\partial}{\partial x_\beta}\left(C_{\alpha\beta\gamma\delta}\,\frac{\partial}{\partial x_\delta}\right) \tag{3.3}$$

where $\{x_\beta\}$ is the four vector (x_1, x_2, x_3, x_4), with x_4 the time coordinate. Further $C_{\alpha\beta\gamma\delta}$ is the "elastic-inertia" tensor defined by

$$C_{\alpha\beta\gamma\delta}\begin{cases} C_{\alpha\beta\gamma\delta} = -C_{ijk\ell};\ \alpha,\beta,\gamma,\delta = 1,2,3 \\ C_{i4k4} = C_{4i4k} = \rho\delta_{ik};\ i,k = 1,2,3 \\ C_{\alpha\beta\gamma\delta} = 0;\ \text{otherwise} \end{cases} \tag{3.4}$$

where $C_{\alpha\beta\gamma\delta}$ has the same symmetry properties as did $C_{ijk\ell}$, that is:

$$C_{\alpha\beta\gamma\delta} = C_{\beta\alpha\gamma\delta} = C_{\alpha\beta\delta\gamma} = C_{\gamma\delta\alpha\beta} \tag{3.5}$$

In addition U_γ and f_α are the "space-like" four vectors defined as

$$\{u_\alpha\} = (u_1, u_2, u_3, 0)$$
$$\{f_\alpha\} = (b_1, b_2, b_3, 0) \tag{3.6}$$

while η_β is a four vector normal (in space-time) with a time like component and is defined by $\{n_\beta\} = (n_1, n_2, n_3, \underline{W}^* \cdot \hat{n})$ where $\underline{W}^*$ is the boundary velocity vector relative to the material particle velocity: $\underline{W}^* = \underline{W} - \underline{V}$. Finally, $\tau_{\alpha\beta}$ is the generalized inertial-stress tensor given by

$$\tau_{\alpha\beta} = C_{\alpha\beta\gamma\delta} \frac{\partial u_\gamma}{\partial x_\delta} \tag{3.7}$$

which has the same formal structure as the ordinary stress tensor T_{ij}, but has the added feature of containing the inertial forces as well.

An equivalent form for the equation of motion is, from 3.2 and 3.3;

$$\tau_{\alpha\beta,\beta} = \rho f_\alpha \tag{3.8}$$

so that the equations of motion can be expressed as the divergence of the symmetric four tensor $\tau_{\alpha\beta}$. This allows a Green's function representation for the displacement field u_γ to be obtained for the general case in which the boundaries of the medium may move with a velocity $\underline{W}$ which is different than the particle velocity.

In the applications of the Green's function solution to be discussed here, we will not be particularly concerned with the cases in which a boundary or boundaries in the medium move with some velocity other than the material particle velocity. However, this feature of the formulation has been used to describe failure boundary growth and the associated radiation of elastic energy in a prestressed medium by Archambeau and Minster [1977].

In any case, Archambeau and Minster [1977] show that Green's function solution of the system 3.2 is given by

$$4\pi u_\mu(\underline{x}) = \int_\Omega \rho f_\alpha G^\mu_\alpha \, d^4x_0 - \int_0^{t^+} dt_0 \int_{\partial\nu_1} J^\mu_\beta \, \eta_\beta \, da^\circ$$

$$+ \int_0^{t^+} \left[d \int_{\nu_1} J^\mu_4 \, d\nu^\circ \right] \tag{3.9}$$

where J^μ_β is the concomitant for u_α and the Green's function $G^\mu_\alpha(\underline{x};\ \underline{x}_0)$ and is given by

$$J^\mu_\beta = G^\mu_\alpha \, \tau_{\alpha\beta} - u_\alpha \, \underset{\sim}{G}{}^\mu_{\alpha\beta} \tag{3.10}$$

where

$$\underset{\sim}{G}{}^\mu_{\alpha\beta} = C_{\alpha\beta\gamma\delta} \frac{\partial G^\mu_\gamma}{\partial x_\delta} \tag{3.11}$$

is the inertial-stress tensor associated with the Green's tensor G^μ_γ.

From the definition of J^μ_β and the associated functions, we have that

$$J^\mu_4 = \rho \left[u_k \frac{\partial G^m_k}{\partial t_0} - G^m_k \frac{\partial u_k}{\partial t_0} \right] \tag{3.12}$$

$$J^4_4 = 0$$

where u_k and G^m_k are Cartesian tensors in the ordinary three-dimensional space.

Further, the various limits of integration appearing in (9) are over Ω, the four-volume in which the time coordinate $x_4 \equiv t$ ranges over the interval $(0, t^+)$ with $t^+ = t + \varepsilon$, with $\varepsilon > 0$ and infintesimal (which is used only to avoid singular points of the Green's function which may occur), while the spatial coordinates range over the ordinary spatial volume V_1. Thus, ∂V_1 denotes the spatial surface of V_1.

If we rewrite the Green's integral solution 3.9, using the original definitions of the various four tensors, we can express (9) in terms of the ordinary spatial three tensors as

$$4\pi u_m(\underline{x},t) = \int_0^{t^+} dt_0 \int_{V_1} \rho(\underline{x}_0)\ f_k(\underline{x}_0,t_0) G_k^m(\underline{x},t;x_0,t_0)dv_0$$

$$+ \int_0^{t^+} dt_0 \int_{\partial V_1} \left[G_k^m(\underline{x},t;\underline{x}_0,t_0) \left\{ C_{ijk\ell}(\underline{x}_0) \frac{\partial u_k}{\partial x_0^j} + \rho \frac{\partial u_k}{\partial t_0} W_\ell \right\} \right.$$

$$\left. - u_k(\underline{x}_0,t_0) \left\{ C_{ijk\ell}(\underline{x}_0) \frac{\partial}{\partial x_0^j} G_i^m(\underline{x},t;\underline{x}_0,t_0) + \rho \frac{\partial G_k^m}{\partial t_0} W_\ell \right\} \right] n_\ell dv^0$$

$$+ \int_0^{t^+} d \left[\int_{V_1} \rho \left\{ u_k(\underline{x}_0,t_0) \frac{\partial G_k^m}{\partial t_0} - G_k^m(\underline{x},t;\underline{x}_0,t_0) \frac{\partial u_k}{\partial t_0} \right\} dv_0 \right]$$

(3.13)

This result is similar to the classical Green's function solution except that terms involving W_ℓ, the velocity of the boundary of V_1 are present in the integral over ∂V_1. These terms are negligible when the boundary moves with the particle

velocity, that is, when the boundary is an ordinary material boundary, but can be large and comparable to the other terms in the integral over ∂V_1 when the boundary is a phase transition boundary. In the applications of the present work we will take all boundaries of V_1 to be material boundaries and will neglect these terms. Archambeau and Minster [1976] discuss the general problem.

The final term in 3.9 and 3.13 represents effects of (generalized) "initial values" of the displacement and velocity fields and the integral representing these effects has been written as a Stieltjes integral since in general it has this form when non-material boundaries are present. Thus, in this respect 3.9 and 3.13 are different from the classical representations, however, again it is not necessary to use this general form for the applications here. For the restricted applications of the present discussion, this term reduces to the classical result which accounts for the ordinary initial values of u_k and $\partial u_k/\partial t$.

For application of 3.9, which has the explicit form given in 3.13, we observe that the original field equations governing u_α and G_α^μ are:

$$L_{\alpha\gamma}\, u_\gamma = \rho f_\alpha$$

$$\tau_{\alpha\beta}\eta_\beta\big|_{\Sigma_1} = \tau_{\alpha\beta}\eta_\beta\big|_{\Sigma_2} \tag{3.14}$$

and

$$L_{\alpha\gamma}\, G_\gamma^\beta = \Delta_\alpha^\beta\,(\underline{x};\underline{x}_0)$$

$$\underset{\sim}{G}{}^\mu_{\alpha\beta}\eta_\beta\big|_{\Sigma_1} = 0 \tag{3.15}$$

Both sets of equations apply to the four-volume Ω. In this case, using the boundary conditions that apply for the fields u_α and G^β_γ in 3.9 we have:

$$4\pi u_\mu(\underline{x}) = \int_\Omega \rho f_\alpha G^\mu_\alpha \, d^4x_0 - \int_0^{t^+} dt_0 \int_{\partial V_1} G^\mu_\alpha \, \tau_{\alpha\beta}\eta_\beta \, da^0$$

$$+ \int_0^{t^+} d\left[\int_{V_1} J^\mu_4 \, dv^0\right] \qquad (3.16)$$

This is a rather simple form in which all field quantities on the right side are generally known since they appear in integrals over the medium boundaries in either space or time (i.e., the latter as initial values at t = 0 ordinarily). When the body force field is negligible or entirely absent and when the medium is in equilibrium initially, then only the second integral over the boundary of V_1 appears in 3.16 and we see from the differential system in 3.14 that the boundary condition provides the necessary specification of $\tau_{\alpha\beta}\eta_\beta$ on the surface ∂V_1. (Here we have used $\Sigma_1 \equiv \partial V_1$ to denote the boundary of V_1 approached from inside V_1 while Σ_2 is the boundary approached from outside V_1.) In particular, $\tau_{\alpha\beta}\eta_\beta$ on ∂V_1 takes on the value $\tau_{\alpha\beta}\eta_\beta|_\Sigma$ which corresponds to the "generalized traction" applied externally to the boundary of V_1. If we neglect the boundary motion relative to other effects as described earlier, then $\tau_{\alpha\beta}\eta_\beta$ reduces to the negative of the ordinary tractions, $t_k \equiv T_{\ell k}n_\ell$ on ∂V_1.

We see from 3.15, however, that we must obtain the Green's function satisfying homogeneous boundary conditions on the boundaries of Ω in order that 3.9 reduce to the simple form 3.16. Often this is difficult and sometimes, of

course, impossible for complicated problems. In this circumstance, we would want to use an approximate procedure involving some Green's function that we can obtain or is known and that is close to that required for a solution. Thus, for general applications for which the system 3.15 may not be soluble in any practical sense we would want to consider a Green's function given by a system of equations which are "close to" 3.15, but which are soluble. There are in fact several approximate procedures that can be followed. One approach is to simply replace the region Ω over which the operator is defined by a new region Ω', which may not contain all the boundaries of Ω but is larger in the sense that all space-time points of Ω are contained in Ω'. Thus, we can introduce a new region Ω' which is such that within this new problem space the equations of 3.15 can be solved for the Green's function. We shall denote these Green's functions by $\Gamma^{\beta}_{\gamma}(\underline{x},\underline{x}_0)$ in 3.9 where 3.9 is still defined over Ω rather than Ω'. Since the Green's function Γ^{β}_{γ} are still defined on Ω then 3.9 has meaning when Γ^{β}_{γ} is used in place of G^{β}_{γ}. However, 3.9 will become an integral equation rather than a solution like 3.16, and while Γ^{β}_{γ} will be known and usually in a relatively simple form, it will now be necessary to solve an integral equation for the unknown field $u_{\mu}(\underline{x})$, by iteration methods for example.

Specifically, we define the class of approximating Green's functions Γ^{β}_{γ} by

$$L_{\alpha\gamma}\Gamma^{\beta}_{\gamma}(\underline{x},\underline{x}_0) = \Delta^{\beta}_{\alpha}(\underline{x},\underline{x}_0);\ \underline{x}\in\Omega' \qquad (3.17)$$

$$\gamma^{\mu}_{\alpha\beta}(\underline{x},\underline{x}_0)\ \eta_{\beta} = 0;\quad \underline{x},\ \underline{x}_0\ \varepsilon\Omega'$$

where

$$\gamma^{\mu}_{\alpha\beta}(\underline{x};\underline{x}_0) = C_{\alpha\beta\gamma\delta}(\underline{x}) \frac{\partial \Gamma^{\mu}_{\gamma}}{\partial x_{\delta}} \tag{3.18}$$

is the inertial-stress tensor associated with Γ^{μ}_{γ}. We assume that Ω' contains Ω but that at least some of the boundaries of Ω are not present in Ω' (e.g., Ω' could be an infinite space, so that the boundary condition in 3.17 would be satisfied at infinity and Ω would be contained in Ω', but Γ^{β}_{γ} would not account for any of the boundaries of Ω).

Now, using 3.9 with Γ^{β}_{γ} gives for $u_{\mu}(\underline{x})$ in Ω:

$$4\pi u_{\mu}(\underline{x}) = \int_{\Omega} \rho f_{\alpha} \Gamma^{\mu}_{\alpha}\, d^3x_0 - \int_0^{t^+} dt_0 \int_{\partial V_1} \Gamma^{\mu}_{\alpha} \left[\tau_{\alpha\beta}\eta_{\beta}\right] da^0$$

$$+ \int_0^{t^+} dt_0 \int_{\partial V_1 \Theta \partial V_1'} u_{\alpha} \left[\gamma^{\mu}_{\alpha\beta}\eta_{\beta}\right] da^0$$

$$+ \int_0^{t^+} d\left[\int_{V_1} J^{\mu}\right] dv^0 \tag{3.19}$$

where $\partial V_1 \Theta \partial V_1'$ is the set theoretic difference in the spatial boundary of V_1 and V_1'. Here V_1 is the purely spatial part of Ω while V_1' is the purely spatial part of Ω'. Clearly, the third term vanishes if the boundaries of Ω coincide with those of Ω. Here we have taken the temporal parts of Ω and Ω' to coincide, so that the time interval for both problems is taken to be $(0, \alpha)$, or in effect $(0, t^+)$ due to the causal properties of the Green's functions.

We observe that since Ω' and Ω do not coincide by definition, then the third term in 3.19, which involves the displacement field u_2 on $\partial V_1 \Theta \partial V_1'$, is normally nonzero. If the choice of Ω' is a good one, in terms of an approximation to the solution for $u_\mu(\underline{x})$ using the proper Green's function, then this term in 3.19 will be small or of no importance in the problem to be solved.

A good approach to the solution of 3.19 when Ω' has been chosen to make the third term relatively small is to take the first iterate to the solution to be the sum of the three other terms in 3.19, which can be computed directly. Thus, we take

$$4\pi u_\mu^I(\underline{x}) = \int_\Omega \rho f_\alpha \Gamma_\alpha^\mu \, d^4x_0 - \int_0^{t^+} dt_0 \int_{\partial V_1} \Gamma_\alpha^\mu \left[\tau_{\alpha\beta} n_\beta\right] da^0$$

$$+ \int_0^{t^+} d\left[\int_{V_1} J_4^\mu \, dv^0\right] \qquad (3.20)$$

As the first approximation to $u_\mu(\underline{x})$; the second approximation is then given by

$$4\pi\left(u_\mu^{II}(\underline{x}) - u_\mu^I(\underline{x})\right) = \int_0^{t^+} dt_0 \int_{\partial V_1 \Theta \partial V_1'} u_\alpha^I(\underline{x}_0) \left[\gamma_{\alpha\beta}^\mu(\underline{x};\underline{x}_0) \, n_\beta\right] da^0$$

(3.21)

with higher order terms given similarly.

These results are essentially the only formal structure that is required to generate representations of the field which will be useful in a number of applications. Some particular relations which amount to alternate expressions of the same representations are, however, useful.

The first of these is the expression of the Green's function representations for $u_\mu(\underline{x})$ in the frequency domain. By taking temporal Fourier transforms of the previous results, we have; using 3.19 which becomes the exact solution given in 3.16 when $\Omega' = \Omega$ and is the appropriate approximation for some choice of Ω .

$$4\pi\tilde{u}_m(\underline{x},\omega) = \int_{V_1} \rho\tilde{f}_k\tilde{\Gamma}^m_k \, dV_0 - \int_{\partial V_1} \tilde{\Gamma}^m_k \, [\tilde{\tau}_{k\ell} \, n_\ell] \, da^0$$

$$+ \int_{\partial V_1 \Theta \partial V'_1} \tilde{u}_k \left[\tilde{\gamma}^m_{k\ell} \, n_\ell\right] da^0 \qquad (3.22)$$

where we have neglected the initial value term involving J^μ_4 since in the following applications we will consider only cases in which the initial condition is an equilibrium condition and where all boundaries are material boundaries.* Further, since we have taken all boundaries to be material boundaries, then all tensors are three tensors and the normal n_ℓ is the ordinary spatial normal on ∂V_1. The notation $\tilde{u}_m$ denotes a Fourier transformed field quantity where:

*Archambeau [1968] gives results for the case in which the initial value term is included, with an application designated to describe failure phenomena.

$$\tilde{u}_m(\underline{x},\omega) = \frac{1}{\sqrt{2\pi}} \int_{-\infty}^{\infty} u_m(\underline{x},t)\, e^{-i\omega t}\, dt \qquad (3.23)$$

Here also $\tilde{\Gamma}_k^m$ is the transform of the two point tensor and is a function of the spatial coordinates $\underline{x}$ and $\underline{x}_0$ alone, while depending parametrically on ω (i.e., the source time t_0 is not present). Examples of these Green's functions in transformed form will be given in a later section along with their time domain expression. Finally, $\tilde{\tau}_{k\ell}$ and $\tilde{\gamma}_{k\ell}^m$ are the negatives of the ordinary stress tensors associated with the fields $\tilde{U}_k$ and $\tilde{\Gamma}_k^m$, respectively.

In addition to the direct expression of the displacement field in terms of the Green's function integral as in 3.19 and 3.22, it is often useful to generate the displacement field from potential fields that satisfy simplier differenetial equations. This can often simplify the analytical problem since we can use the much simplier Green's functions for the potentials in an integral Green's function relation that gives the potentials everywhere in terms of their boundary values and then obtain the displacement fields, stress fields, etc. for the entire region using the differential relation between the displacement field and the potentials.

Specifically, we may define potentials χ_α, $\alpha = 1, 2, 3, 4$ such that [Archambeau; 1968, 1972]:

$$\frac{\partial^2 U_k}{\partial t^2} = v_p^2 \frac{\partial \chi_4}{\partial x_k} - 2v_s^2 \left[\varepsilon_{k\ell m} \frac{\partial \chi_m}{\partial x_\ell}\right] + f_k \qquad (3.24)$$

where the four χ_α are the three components of the rotation ($\alpha = 1, 2, 3$) and the dilatation ($\alpha = 4$) so that:

$$\chi_k = \frac{1}{2}\,\epsilon_{k\ell m}\,\frac{\partial U_m}{\partial x_\ell}\;;\quad \chi_4 = \frac{\partial U_\ell}{\partial x_\ell} \tag{3.25}$$

with $\epsilon_{k\ell m}$ the alternating tensor. Equation 3.24 is just the equation of motion for the medium under the conditions of isotropy and homogeneity. That is, it corresponds to Eq. 3.1 when we take the elastic tensor, $C_{ijk\ell}$, to be

$$C_{ijk\ell} = \lambda\delta_{ij}\,\delta_{\ell k} + \mu\,(\delta_{i\ell}\,\delta_{jk} + \delta_{ik}\,\delta_{j\ell}) \tag{3.26}$$

with λ, μ and ρ in 3.1 to be constants. In many applications this is an adequate (local) representation for the medium.

Using 3.24, it is easy to show that the individual potentials satisfy wave equations by taking, successively the curl and divergence of this equation. We have, therefore, that:

$$\nabla^2\chi_\alpha - \frac{1}{v_\alpha^2}\,\frac{\partial^2}{\partial t^2}\,\chi_\alpha = -4\;q_\alpha \tag{3.27}$$

where

$$v_\alpha \equiv (v_s,\ v_s,\ v_s,\ v_p)$$

$$q_\alpha = \begin{pmatrix} \dfrac{1}{2v_s^2}\,\epsilon_{k\ell m}\,\dfrac{\partial f_m}{\partial x_\ell} \\[2ex] \dfrac{1}{v_p^2}\,\dfrac{\partial f_m}{\partial x_m} \end{pmatrix};\ k = 1,2,3$$

If we consider temporal Fourier transformed fields, then we have

$$u_k = -\frac{1}{k_p^2}\frac{\partial \tilde{\chi}_k}{\partial x_k} + \frac{2}{k_s^2}\varepsilon_{k\ell m}\frac{\partial \tilde{\chi}_m}{\partial x_\ell} - \frac{1}{\omega^2}\tilde{f}_k \tag{3.28}$$

in place of 3.24 and

$$\nabla^2\tilde{\chi}_\alpha + k_\alpha^2\,\tilde{\chi}_\alpha = \tilde{q}_\alpha \tag{3.29}$$

in place of 3.27 , where:

$$\tilde{\chi}_\alpha = \frac{1}{\sqrt{2\pi}}\int_{-\infty}^{\infty} \chi_\alpha\,(\underline{x},t)\;\ell^{-i\omega t}\,dt \tag{3.30}$$

and $k_\alpha = \omega/v_\alpha = (k_s,\ k_s,\ k_s,\ k_p)$.

Thus, we see that each of the four potentials satisfied an equation of the same form, namely a scalar wave equation, and that if we solve for the χ_α then we can construct the acceleration, velocity, displacement and stress fields from them. Naturally, the boundary conditions on the χ_α are just those given for example in 3.2 and must, of course, be taken into account.

Now the Green's function integral representations for the χ_α are quite simple and in addition, the scaler Green's functions, which satisfy differential equation of the form

$$\nabla^2 G(\underline{r},t;\underline{r}_0,t_0) - \frac{1}{v^2}\frac{\partial^2}{\partial t^2}G(\underline{r},t;\underline{r}_0,t_0)$$

$$= -4\pi\delta(\underline{r}-r_0)\,\delta(t-t_0) \tag{3.31}$$

is also relatively simple compared to the tensor Green's function associated with u_m.

In particular, the Green's function integral giving any of the potentials χ_α is [e.g., Morse and Feshbach, 1953].

$$4\pi\chi(\underline{r},t) = \int_0^{t^+} dt_0 \int_{V_1} G\, q\, dv_0 + \int_0^{t^+} dt_0 \int_{\partial V_1} \{G\nabla\chi - \chi\nabla G\} \cdot \hat{n}\, da^0 \qquad (3.32)$$

where we have suppressed the index α denoting the individual potentials since they all have solutions of identical formal structure, with v, G, χ and q having the appropriate index depending on which χ_α is represented. where all initial value terms for the potentials χ_α have been taken to be zero. Results applying when initial values are to be accounted for or when moving boundaries are involved are given, for example, by Minster, 1973.

Analogously with 3.22, we have the representation in the frequency domain

$$4\pi\tilde{\chi}(\underline{r},\omega) = \int_{V_1} \rho\tilde{q}\tilde{G}\, dV_0 + \int_{\partial V_1} \left[\tilde{G}\, \nabla_0\tilde{\chi} - \tilde{\chi}\nabla_0\tilde{G}\right] \cdot \hat{n}\, da^0 \qquad (3.33)$$

where the initial value terms are again taken to be zero in this result, as was done for 3.32.

In both 3.32 and 3.33, we have not introduced any special notation for approximating scaler Green's functions corresponding to the earlier use of Γ_k^m as an approximating Green's function, since in defining G and generating the

integral solutions we have not made explicit use of the boundary conditions for χ and G on ∂V_1. Hence, we can think of the G appearing in these results as being defined on some region $\Omega' \subset \Omega$, where Ω' may be identical with Ω as a special case. In general, as with the previous results involving u_m directly, Ω' will not be the same as Ω. And the Green's function in 3.32 and 3.33 will be an approximating Green's function. Consequently, the solution of the resulting integral equations for the χ_α would preceed in the same manner as was indicated earlier for u_m; where we used an iterative approach.

Eigenfunction Expansions: Multipole Field Representations of Source Radiation Fields. As a first application of the Green's function representations of the previous section, consider the case in which the dynamic field from a localized energy source has been computed by a purely numerical procedure, or is known by some other means. For example, suppose we compute the motion of the medium due to a large explosion, with the region in the immediate vicinity of the explosion behaving nonlinearly in response to the high amplitude shock wave. At some distance from the source the stress wave will, however, decay to the point where the medium behaves linearly. At this point the wave field will obey the linearized equations of motion (1). Thus we may view the subsequent response of the medium in the linear region V_1, exterior to this nonlinear zone, as being a consequence of impressed field values (e.g., tractions) on the boundary of V_1 as indicated in Figure 3.1 (i.e., essentially this is just the Cauchy stress principle). In fact, we need not be concerned with what occurs in the region V_2 (Figure 3.1) but only with the values of the field on the boundary ∂V_1.

Now if we wish to represent the field propagating into V_1 due to the impressed field on the boundary ∂V_1, then we may use the Green's function solutions given in Section I directly. In particular, we can assume that the initial values of the field in V_1 are zero, that there are no external time varying body forces, and that we do not have any complications involving moving boundaries having rates different from the particle velocities. Then we have for the displacement field in V_1

$$4\pi u_m(\underline{x},t) = \int_0^{t^+} dt_0 \int_{\partial V_1} \left\{ \Gamma_\ell^m \, (T_{\ell k}\eta_k) - \ell\left(\gamma^m_{\ell k}\eta_k\right)\right\} da^\circ \qquad (3.34)$$

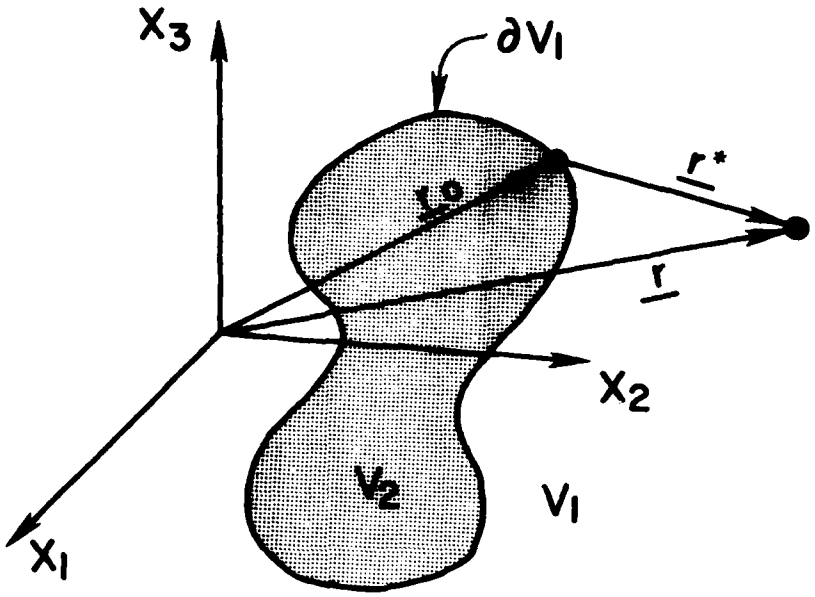

Figure 3.1: Schematic of the elastic region V_1, where field values are known on the boundary ∂V_1. V_2 may be a linear elastic or nonlinear zone, but ∂V_1 must be within the elastic zone.

Here $T_{\ell k}\eta_k = t_\ell$ are the tractions and u_ℓ the displacements on ∂V_1, which are assumed specified for example, by the numerical calculation in V_2 and given over the time interval in which they are non-zero. Now we may use the infinite space Green's function Γ_ℓ^m in 3.34 to calculate $_m(\underline{x}, t)$ in V_1.

If, in particular, we expand the Green's function Γ_ℓ^m and the traction $\gamma_{\ell k}^m \eta_k$ derived from it in terms of vector spherical wave functions, then $u_m(\underline{k},t)$ can be expressed as an expansion in terms of these functions. In this case $u_m(\underline{x},t)$ will be expressed in terms of a vector multipole expansion about some origin point which can be taken arbitrarily. If we choose the origin at a point within V_2 corresponding to a natural symmetry point for the source of the radiation field we can consider this resulting expanded wave field as an equivalent point source which gives the same radiation field in V_1 as does the process occurring in V_2. (It does not, of course, give the actual radiation field within V_2 itself, but simply gives the analytically continued field from V_1 into V_2.)

The expansion of the Green's tensor in terms of eigenfunctions can be accomplished in one, two or three dimensions for the medium with boundaries, so that the region V_1 could be layered, for example, and the Green's function expansion would be in terms of the eigenfunctions for the layered medium. Thus we can build in the effects of medium boundaries in the expansion for $U_m(\underline{\alpha},t)$ in V_1. For example, if the space were a half space or a spherical region and V_2 (the "source" volume) was near or intersected the outer boundary of the space, we would use an eigenfunction expansion for Γ_ℓ^m involving half space or spherical wave functions that satisfied the boundary condition on the medium external boundary.

Finally we note that 3.34 applies to one, two or three dimensional problems where ∂V_1 is to be interpreted in general as the boundary of the space, so that if the problem is two-dimensional, then ∂V_1 is a curve. Then use of the Green's function appropriate to the dimensionality of the space gives the representation of u_m.

We can also represent u_m in the frequency domain using previous integral results. We have as the frequency domain version of 3.34 from 3.22 :

$$4\pi \tilde{u}_m(\underline{x},w) = \int_{\partial V_1} \left\{ \tilde{\Gamma}^m_{\ell}\left(\tilde{T}_{\ell k}\eta_k\right) - \tilde{u}_{\ell}\left(\tilde{\Gamma}^m_{\ell k}\eta_k\right)\right\} da^{\circ} \quad (3.35)$$

This representation can be used in the same way as , but is somewhat simpler to use since the Green's function eigenfunction expansions for the space are easier to obtain and express in the frequency domain than are those for the time domain.

With regard to simplifying the analytical procedures required by 3.34 and 3.34 in order to express u_m in V_1 as a multipolar (or eigenfunction) expansion, it is often appropriate to generate the potentials χ_α in V_1 from known values on the boundary ∂V_1. Then, of course u_m and associated fields can be calculated in V_1.

Thus, if we choose to use the χ_α for the representation, then we have that χ_α in V_1 is given by:

$$4\pi\chi_\alpha(\underline{r},t) = \int_0^{t^+} dt_0 \int_{\partial V_1} \left\{ G\nabla_0\chi - \chi\nabla_0 G\right\} \cdot \hat{n}\, da^{\circ} \quad (3.36)$$

from Eq. (32). In the frequency domain we have

$$4\pi\tilde{\chi}_\alpha(r,\omega) = \int_{\partial V_1}\left[\tilde{G}\nabla_0\tilde{\chi}-\tilde{\chi}\nabla_0\tilde{G}\right]\cdot\hat{n}\,da' \qquad (3.37)$$

We then can use 3.27 or 3.28 to obtain the displacement field. Equations 3.36 and 3.37 have the same structure as do the more complex equations 3.34 and 3.35, but are more restricted in that these results are obtained for the case of a homogeneous, isotropic medium whereas 3.34 and 3.35 are general in this respect. Nevertheless, we may consider the region V_2 (the "source" region) to be, to a reasonable approximation in most instances, confined to a homogeneous isotropic medium "layer" or subregion. In this case V_1 is only the region within this layer and 3.36 and 3.37 given only the field in this subregion. To obtain the field in the whole space occupied by the (layered) medium we must adjoin this subregion field representation to eigenfunction expansions in the other layers or subregions; this process of connecting subregion solutions or eigenfunction expansions is accomplished in the usual way by applying boundary conditions at the subregion interfaces (continuity conditions). Hence the restriction of 3.36 and 3.37 to a subspace of the whole space does not generally reduce the usefulness of the expansion procedure implied by these results.

One important result arises when V_2 can be considered to occupy only one subregion of the entire medium in which the material properties are essentially constant and, as a consequence, that V_1 can also be considered to be the extension of this homogeneous zone. Then we can use the infinite space Green's function for $\tilde{G}$ in V_1 to generate $\tilde{\chi}_\alpha$. We have in this case, using the Green's function expansion in spherical eigenfunctions in a whole space:

$$\tilde{\chi}_\alpha(\underline{r},\omega) = \sum_{\ell=0}^{\infty}\sum_{k=0}^{\ell}[A_{\ell k}\cos m\phi + B_{\ell k}\sin m\phi] \cdot P_\ell^k(\cos\theta)\, h_\ell^{(2)}(k_\alpha r) \tag{3.38}$$

$$\begin{pmatrix} A_{\ell k}(\omega) \\ B_{\ell k}(\omega) \end{pmatrix} = -ik_\alpha\left[\frac{(2\ell+1)}{4\pi}\right]C_{\ell k}\int_{\partial V_1}\left[\nabla\tilde{\chi}_\alpha\cdot\hat{n}\right]P_\ell^k(\cos\theta_0)\begin{pmatrix}\cos k\phi_0 \\ \sin k\phi_0\end{pmatrix} j_\ell(k_\alpha r_0) - \tilde{\chi}_\alpha\left[\nabla_0\left\{P_\ell^k(\cos\theta_0)\begin{pmatrix}\cos k\phi_0 \\ \sin k\phi_0\end{pmatrix}j_\ell(k_\alpha r_0)\right\}\cdot\hat{n}\right]da^\circ \tag{3.39}$$

Here

$$C_{\ell k} = (2-\delta_{k_0})\,\frac{(\ell-k)!}{(\ell+k)!}$$

We may, of course, take ∂V_2 to be a spherical surface enclosing V_2, but this is not necessary and ∂V_1 can be any convenient surface enclosing V_2.

In case V_2 and V_1 intersect an external boundary of the medium (a free surface) then an appropriate appraoch is to use a half space Green's function representation. This can be accomplished by using a Green's function expansion in eigenfunctions for the half space, or by use of an image source, etc.

If we use the time domain representation 3.36 rather than 3.37 to represent the field, then

$$4\pi\chi_\alpha(\underline{r},t) = \int_0^{t^+} dt_0 \int_{\partial V_1}\left\{G\nabla_0\chi - \chi\nabla_0 G\right\}\cdot\hat{n}\, da^\circ \tag{3.40}$$

When the infinite space Green's function can be approximately used, then we have:

$$4\pi\chi_\alpha(\underline{r},t) = \int_0^{t^+} dt_0 \int_{\partial V_1} da^\circ \left\{ \frac{\delta(t_0 - t + r^*/v_\alpha)}{r^*} \nabla_0 \chi_\alpha \cdot \hat{n} \right.$$

$$\left. - \chi_\alpha \nabla_0 \left[\frac{\delta(t_0 - t + r^*/v_\alpha)}{r^*} \right] \cdot \hat{n} \right\} \qquad (3.41)$$

However, we have, interchanging the integrations over t_0 and ∂V_1, that

$$\int_0^{t^+} \frac{1}{r^*} \delta(t_0 - t - r^*/v_\alpha) \nabla_0 \chi_\alpha(\underline{r}_0, t_0) \, dt_0 = \frac{1}{r^*} \nabla_0 \chi_\alpha(\underline{r}_0, t - r^*/v_\alpha)$$

$$\int_0^{t^+} \chi_\alpha \nabla_0 \left[\frac{\delta(t_0 - t + r^*/v_\alpha)}{r^*} \right] dt_0$$

$$= \int_0^{t^+} \chi_\alpha \frac{\partial}{\partial r^*} \left[\frac{\delta(t_0 - t + r^*/v_\alpha)}{r^*} \right] \nabla_0 r^* \, dt_0$$

$$= \int_0^{t^+} \chi_\alpha \frac{\hat{r}^*}{(r^*)^2} \left[-\delta(t_0 - t + r^*/v_\alpha) + \frac{r^*}{v_\alpha} \delta'\left(t_0 - t + \frac{r^*}{v_\alpha}\right) \right] dt_0$$

$$= - \frac{\hat{r}^*}{(r^*)^2} \left\{ \chi_\alpha(\underline{r}_0, t - r^*/v_\alpha) + \frac{r^*}{v_\alpha} \left[\frac{\partial}{\partial t_0} \chi_\alpha \right]_{t_0 = t - r^*/v_\alpha} \right\}$$

where $\hat{r}^*$ is the unit vector in the direction from a source point to the receiver point (see Figure 1).

Hence, we have:

$$4\pi\chi_\alpha(\underline{r},t) = \int_{\partial v_1} \left[\frac{1}{r^*}\nabla_0\lambda_\alpha + \left(\frac{\hat{r}^*}{r^{*2}}\right)\chi_\alpha - \left(\frac{\hat{r}^*}{v_\alpha r^*}\right)\frac{\partial\chi^\alpha}{\partial t_0}\right]_{t_0=t-r^*/v_\alpha} \cdot \hat{n}\, da^o \qquad (3.42)$$

Thus, with $\nabla_0\chi_\alpha$, χ_α and $\partial\chi_\alpha/\partial t_0$ specified (numerically or otherwise) on ∂v_1 where this surface may be chosen arbitrarily so long as it encloses v_2, we can compute χ_α in v_1 in the time domain. Methods of integration of 3.42 using expansions of $1/r^*$, in terms of spherical eigenfunctions are straightforeward (e.g., see Archambeau, 1968).

The same procedure of integration over t_o which leads to 3.42 can also be applied to 3.34, the Green's integral representation of $u_m(\underline{x},t)$, using the Green's tensor.

To summarize the approach outlined in this application, we observe that the Green's function integral representation provides us with a method of representing the field in the elastic zone in analytic terms when the field is specified on the boundary of the elastic zone. This representation, therefore, provides us with a way of representing a nonlinear source of energy by a linear (elastic) equivalent source that gives us the identical field in the elastic zone surrounding the complex (nonlinear) source zone. Further, it gives an expression for this field in an analytic form which is appropriate for the analysis of the further propagation of this source field in the complex (layered) elastic medium surrounding the source.

Application to Numerical Problems: Transparent Grid Boundaries. We can easily make use of the previous results to show how a numerical grid boundary can be made "transparent" to the propagation of elastic waves. We will treat the simple case involving potentials χ_α here to illustrate the method.

In particular, consider ∂V_1 to be the boundary defined by the grid points at one grid spacing within the grid system as shown in Figure 3.2. Let V_2 be the grid region. Now we wish to treat the region exterior to V_2 (and within V_1 therefore) to be an infinite space so that in this case the points on the actual grid boundary are in V_1 and so will transmit energy as if they were in an infinite space rather than as the terminal points of a numerical grid. To do this we are merely required to predict the fields at the grid boundary points $B_g \subset V_1$ using the values of the fields specified on ∂V_1 in an infinite space Green's function integral representation. If we do this, then the boundary of the grid will deform as if it were in an infinite space rather than at the termination points of the grid and no energy will be reflected back into the numerical grid.

Using the potentials $\chi_\alpha(\underline{r},t)$ we observe that the fields at the grid boundary are given by 3.42, where we set $\underline{r} = \underline{r}_g$ as the coordinate vector of points on B_g. Further, replacing r* by R_g where

$$R_g = |\underline{r}_g - \underline{r}_0|$$

where $\underline{r}_0$ are the "source" points on ∂V_1 in 3.42, then we have for the potentials on B_g:

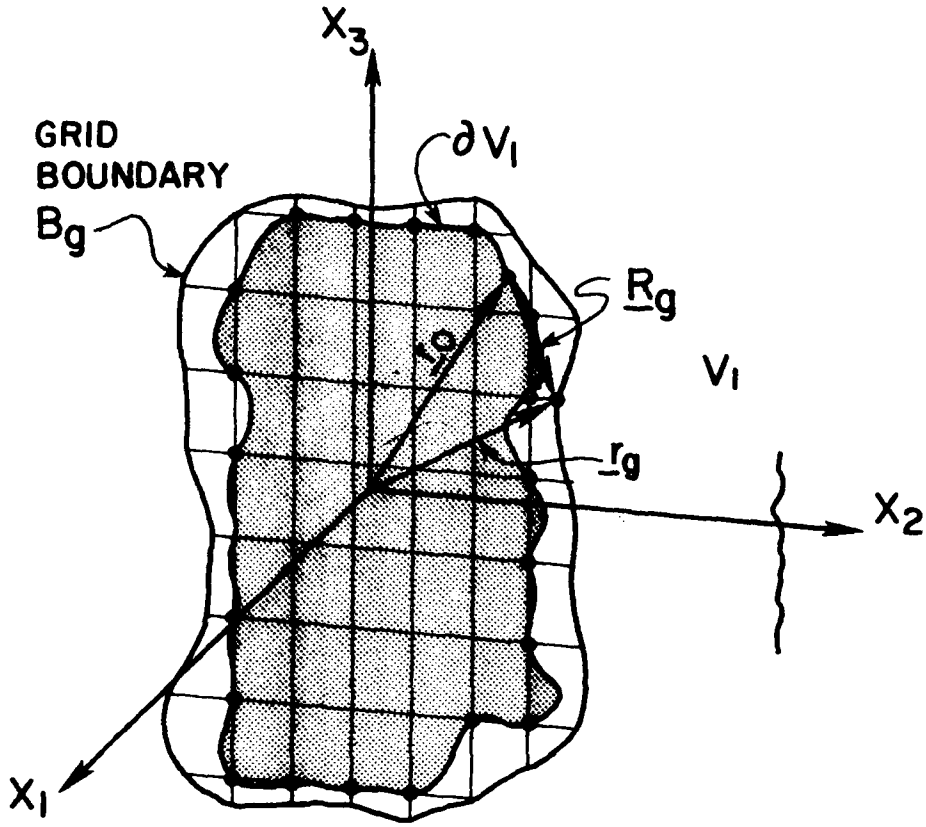

Figure 3.2: Numerical grid over the region V_2 with ∂V_1 corresponding to the surface at one grid spacing inside the grid boundary. ∂V_1 is viewed as the boundary to an external infinite space, where fields are defined by a Green's function integral.

UNCLASSIFIED

SECURITY CLASSIFICATION OF THIS PAGE (When Data Entered)

REPORT DOCUMENTATION PAGE		READ INSTRUCTIONS BEFORE COMPLETING FORM
1. REPORT NUMBER Semi-Annual Technial Report No. 5	2. GOVT ACCESSION NO. AD-A123476	3. RECIPIENT'S CATALOG NUMBER
4. TITLE (and Subtitle) Earthquake Characteristics and Earthquake-Explosion Discrimination		5. TYPE OF REPORT & PERIOD COVERED Semi-Annual Technical Report 1 Nov 1976-30 Apr 1977 6. PERFORMING ORG. REPORT NUMBER
7. AUTHOR(s) C. Kisslinger, C.B. Archambeau, V.F. Cormier, G. Lundquist, C. Salvado, J. Stevens		8. CONTRACT OR GRANT NUMBER(s) AFOSR-75-2775
9. PERFORMING ORGANIZATION NAME AND ADDRESS CIRES University of Colorado Boulder, Colorado 80309		10. PROGRAM ELEMENT, PROJECT, TASK AREA & WORK UNIT NUMBERS ARPA Order 3291 Program Code 7F10 Program Element 62701E
11. CONTROLLING OFFICE NAME AND ADDRESS Advanced Research Projects Agency /NMR 1400 Wilson Boulevard Arlington, Virginia 22209		12. REPORT DATE 30 April 1977 13. NUMBER OF PAGES 81 pages
14. MONITORING AGENCY NAME & ADDRESS (if different from Controlling Office) Air Force Office of Scientific Research/NP Bolling Air Force Base, Bldg 410 Washington, D.C. 20332		15. SECURITY CLASS. (of this report) UNCLASSIFIED 15a. DECLASSIFICATION/DOWNGRADING SCHEDULE

16. DISTRIBUTION STATEMENT (of this Report)

Approved for public release; distribution unlimited.

17. DISTRIBUTION STATEMENT (of the abstract entered in Block 20, if different from Report)

18. SUPPLEMENTARY NOTES

19. KEY WORDS (Continue on reverse side if necessary and identify by block number)

wave amplitudes	inelastic attenuation
seismic spectra	m_b:M_s
Langer approximation	tectonic stress
synthetic seismograms	numerical calculations of wave fields

20. ABSTRACT (Continue on reverse side if necessary and identify by block number)

A full-wave theory applicable to the synthesis seismograms at distances 10° to 40°, for an upper mantle with either first-order discontunuities or rapid but continuous changes in properties has been developed. The effects of steep gradients on wave amplitudes is demonstrated. A frequency-dependent Q model has been applied to the analysis of spectra of body-wave from shallow and deep earthquakes. Evidence for Bulk losses, apparently concentrated in the asthenosphere, has been found. The Green's function

DD FORM 1 JAN 73 1473 EDITION OF 1 NOV 65 IS OBSOLETE

UNCLASSIFIED

SECURITY CLASSIFICATION OF THIS PAGE (When Data Entered)

representation of a wave field has been used to develop an efficient technique for computing the far-field radiation from a non-linear source region. A method of effecting a transparent grid boundary for numerical wave-field conculations has also been developed.